D 432037

U.S. DEPARTMENT OF COMMERCE

PB80-171317

Effects of Moisture, Residual Thermal Curing Stresses and Mechanical Load on the Damage Development in Quasi-Isotropic Laminates

Virginia Polytechnic Inst. and State Univ.
Blacksburg

Prepared for

National Aeronautics and Space Administration
Hampton, VA. Langley Research Center

Feb 80

COLLEGE OF ENGINEERING

VIRGINIA POLYTECHNIC INSTITUTE AND STATE UNIVERSITY

BLACKSBURG, VIRGINIA

College of Engineering
Virginia Polytechnic Institute and State University
Blacksburg, VA. 24061

VPI-E-80-5 February, 1980

Effects of Moisture, Residual Thermal Curing Stresses and Mechanical Load on the Damage Development in Quasi-Isotropic Laminates

Ronald D. Kriz[1]

Wayne W. Stinchcomb[2]

Darrel R. Tenney[3]

Department of Engineering Science and Mechanics

Interim Report Number 16
NASA-Virginia Tech Composites Program

NASA Grant NGR 47-004-129

Prepared for: Materials Application Branch
National Aeronautics & Space Administration
Langley Research Center
Hampton, VA. 23665

[1]Former Graduate Student
[2]Associate Professor
[3]Materials Engineer - NASA Langley

BIBLIOGRAPHIC DATA SHEET	1. Report No. VPI-E-80-5	2.	3. Recipient's Accession No. PB80 171317
4. Title and Subtitle EFFECTS OF MOISTURE, RESIDUAL THERMAL CURING STRESSES AND MECHANICAL LOAD ON THE DAMAGE DEVELOPMENT IN QUASI-ISOTROPIC LAMINATES			5. Report Date February, 1980 6.
7. Author(s) R. D. Kriz, W. W. Stinchcomb and D. R. Tenney			8. Performing Organization Rept. No. VPI-E-80-5
9. Performing Organization Name and Address Virginia Polytechnic Institute and State University Engineering Science and Mechanics Blacksburg, Virginia 24061			10. Project/Task/Work Unit No. 11. Contract/Grant No. NASA NGR 47-004-129
12. Sponsoring Organization Name and Address National Aeronautics & Space Administration Langley Research Center Hampton, Virginia 23665			13. Type of Report & Period Covered 14.
15. Supplementary Notes			
16. Abstracts See page ii			
17. Key Words and Document Analysis. 17a. Descriptors composite materials, graphite/epoxy, fatigue, moisture, thermal stresses, characteristic damage state 17b. Identifiers/Open-Ended Terms 17c. COSATI Field Group			
18. Availability Statement Distribution unlimited.		19. Security Class (This Report) UNCLASSIFIED 20. Security Class (This Page) UNCLASSIFIED	21. No. of Pages 22. Price

EFFECTS OF MOISTURE, RESIDUAL THERMAL CURING STRESSES AND MECHANICAL LOAD ON THE DAMAGE DEVELOPMENT IN QUASI-ISOTROPIC LAMINATES

ABSTRACT

This investigation demonstrates how the maximum moisture absorbed (that is the "wet" condition) in $[0/\pm45/90]_s$ and $[0/90/\pm45]_s$ laminates fabricated from T300/5208 significantly alters the dry stress state and subsequent damage development along the laminate free edge.

Emphasis is placed on using reasonable approximations for wet, dry, and out-of-plane (ν_{23},G_{23}) elastic properties since these properties are required to predict the damage free stress state at the laminate edge. Classical laminate theory and a finite element model were used to predict stress states prior to the first formation of damage. Crack patterns characteristic of the laminate in a wet or dry condition were also predicted using a shear lag model. Development of edge damage was recorded and observed during the test by transferring an image of the damage from the edge surface on to a thin acetate sheet (replica technique), such that the damage imprinted on the acetate sheet could be immediately viewed on a microfiche card reader.

Moisture was shown to significantly alter the interior and edge dry stress states due to swelling and a reduction of elastic properties. Moisture also reduces the transverse strength in the 90° plies such that the first formation of damage in a wet $[0/\pm45/90]_s$

laminate is a simultaneous occurrence of delaminations and transverse cracks in the 90° plies. A model was developed in order to predict changes in first ply failure laminate loads due to differences in stacking sequence together with a wet or dry environmental condition.

Although moisture was shown to significantly alter the first formation of damage, the crack patterns prior to fracture were not significantly altered by moisture absorption. Consequently, differences between wet and dry laminate static or residual experimental strengths were small.

ACKNOWLEDGEMENTS

This document represents a portion of the work accomplished under NASA Grant NGR 47-004-129 and NASA Cooperative Agreement NCCI-15 during the period September, 1976 through December, 1979. Appreciation is gratefully extended to E. G. Henneke, C. T. Herakovich and K. L. Reifsnider for many valuable discussions and to Frances Carter for excellence in typing and patience in preparing the tables.

TABLE OF CONTENTS

LIST OF FIGURES

LIST OF TABLES

I. INTRODUCTION

Recent emphasis on environmental degradation of graphite/epoxy fiber-reinforced composites is due to the increased use of these high performance materials in aerospace structural applications. It is well established that atmospheric moisture which is absorbed by diffusion into the epoxy matrix degrades those lamina properties which are matrix dependent [1]. The accumulative moisture absorbed by T300/5208 graphite/epoxy when exposed to in-service environments [2] is significant in terms of reduced lamina properties.

Hygrothermal degradation of graphite/epoxy could be attributed to degradation of the fiber, matrix, or fiber/matrix interface. It is generally accepted that fiber properties are unaffected by moisture [1] since moisture has little effect on lamina properties which are fiber dominated. The fiber/matrix interface strength is reduced due to moisture [3]. This can be attributed to a combination of fiber/matrix chemistry [4] (i.e. graphite fiber sizing) and a residual stress state at the graphite/epoxy interface [5]. It is therefore generally accepted that most cracks which result from a mechanically applied load in graphite/epoxy materials initiate at the fiber/matrix interface. When moisture is absorbed overall degradation of the matrix exists since most epoxy resins are susceptible to plasticization, enhanced viscoelastic response, together with a reduction in glass transition temperature, ultimate strength, and stiffness properties [1,6].

Degradation of the epoxy matrix and fiber/matrix interface is

the result of volumetric diffusion [7] of water molecules which attach themselves as hydrogen bonded molecules onto the long epoxy polymer chains. This diffusion increases the epoxy "free volume" [1] which results in swelling. The rate of moisture absorbtion can be conveniently accelerated by exposure at elevated temperatures. Unfortunately accelerated moisture absorption will produce matrix cracking if the temperature exceeds the glass transition temperature [8]. This matrix damage is usually near the surface and is attributed to a combination of matrix plasticization and a residual stress state which is created when a large gradient in moisture concentration profiles causes the dry surface to shrink upon desorption [9]. Although there are many more interesting damage mechanisms which explain the formation of cracks in epoxy resins, many of these mechanisms are worst cases of laboratory induced degradations. Once these worst case damage mechanisms are understood they are usually eliminated from a materials application viewpoint.

Although it is instructive to study these worst case mechanisms, the emphasis in this study is to choose a material system which minimizes these worst case cracking events. Eliminating these worst case events results in a less complex model which can then be used to explain how damage developes in an environmentally conditioned laminate when a mechanical load is applied. Crossman [10] demonstrated that the strength and elastic properties of quasi-isotropic laminates fabricated from T300/5208 were reduced when moisture was absorbed (that is, the "wet" condition), and that no damage resulted from the

absorption of moisture. Crossman also showed that the viscoelastic response of the wet T300/5208 laminates was negligible when compared to the viscoelastic response of wet T300/5209 laminates. This is partially due to the lower glass transition temperature of T300/5209. In summary quasi-isotropic laminates fabricated from T300/5208 will behave elastically in either the wet or dry state such that wet lamina strength and elastic properties are lower than the dry properties and no cracks result when T300/5208 laminates absorb moisture. It follows that the formation of any cracks in a quasi-isotropic laminate fabricated from T300/5208 will be the result of an applied mechanical load acting together with the residual hygro-thermal stress state.

Since wet or dry quasi-isotropic laminates fabricated from T300/5208 behave elastically, the interior in-plane stress state existing prior to the initial formation of damage can be calculated from classical laminate plate analysis using wet or dry elastic properties. Using a laminated plate analysis Kim and Hahn [11] predicted the stress state in a wet and dry $[0/+45/-45/90]_s$ laminate fabricated from T300/5208 prior to formation of the first 90° ply crack. Good correlation between experimental and predicted first 90° ply failure stress in both wet and dry conditions was demonstrated by using averaged wet and dry elastic lamina properties. In Kim's model the wet residual stress state was assumed zero after absorbing 1.3 percent moisture (by weight gained) which implies that all damage is due to a state of stress resulting only from an applied load. The first ply failure loads were predicted using a stress failure criterion along with the laminate

stress state predicted by laminated plate analysis using constant coefficients of expansion.

The stress state in finite width quasi-isotropic laminates is not uniform through the width as assumed by classical laminated plate analysis. Three dimensional stress analysis demonstrates that the stress components which are acting perpendicular to the thin quasi-isotropic laminate plane are negligible away from the free edge but can exceed ply strengths within a thin boundary layer near the free edge [10]. These out-of-plane stresses are the result of a mismatch of Poisson's ratios and coefficients of thermal expansion for each layer in the laminate when loaded mechanically or thermally. The magnitude of the out-of-plane tensile stresses near the free edge can cause interply cracks [12] which are called delaminations. No delaminations occur when the stacking sequence is altered to give compressive out-of-plane stresses. Depending on the stacking sequence the damage which develops along the free edge of the laminate when loaded can be a combination of delaminations between layers or transverse cracks within layers. Previous studies [13] have demonstrated that the damage which develops along the free edge of a $[0/+45/-45/90]_s$ laminate (type I) is entirely different from the free edge damage for a $[0/90/+45/-45]_s$ laminate (type II). Differences in damage states observed along the free edge can ultimately influence the final laminate strength. For type I and type II laminates fabricated from T300/5208 there can be as much as 30 percent difference in dry laminate strengths [14,15]. Therefore, when considering damage leading

to final laminate failure, the emphasis changes from individual transverse cracks to the development of an entire damage state near the free edge prior to failure. In this investigation only damage at the laminate free edge is investigated. No attempt was made to investigate damage away from the free edge.

Due to the heterogeneous nature of fiber-reinforced laminates the damage which develops in a laminate when loaded is a composition of interply delamination cracks and cracks within individual plies which grow transverse, longitudinal, or at an angle to the load axis. Unlike the single critical crack in homogeneous materials, each crack which exists in a heterogeneous laminate cannot be evaluated as an isolated event which grows in a self-similar fashion. Instead, each crack in a heterogeneous laminate is a component of a damage state, and the laminate response is influenced more by the development of this damage state than by the behavior of a single crack.

Based on extensive experimental data, Reifsnider et al [16] have shown that different crack types consistently develop into a stable pattern or "damage state" which is characteristic of the laminate. A rational mechanistic approach can be used to predict a stable pattern of cracks in the off-axis plies prior to laminate failure [17]. This characteristic damage state (CDS) could be used to define the stress and state of strength prior to laminate failure. Recent observations [17] strongly suggest that the CDS could be independent of load history and that the CDS is a laminate property. In summary, the philosophy of CDS is best stated by Reifsnider and Masters [17],

"From the standpoint of mechanics, the CDS has the same significance as the single crack for homogeneous materials in the sense that it is the well-defined damaged physical state from which the fracture event develops."

As already discussed, previous investigations have shown that the formation of damage in quasi-isotropic laminates depends on material, stacking sequence, residual curing stresses, and environmental conditioning. In particular the present investigation is primarily concerned with the effect of residual cure stresses, swelling due to moisture absorption, and mechanical loads on the CDS in type I and type II laminates fabricated from T300/5208 graphite/epoxy. The objectives of this study are to initially isolate unique free edge damage states in type I and type II laminates and show how these unique damage states develop into the CDS when the laminate is mechanically loaded.

Unique free-edge damage states in quasi-isotropic laminates are obtained experimentally by environmentally conditioning type I and type II laminates. The differences in the laminate wet and dry damage free stress states uniquely influence the free edge damage which develops when the laminates are mechanically loaded. While the laminate load is held constant, damage along the free edge is recorded by replicating an image of damage from the free edge surface on to the surface of an acetate strip. Analytic models which predict the state of stress prior to the formation of damage and the characteristic spacing of ply cracks along the free edge are compared with the damage

recorded on the replicas while the laminates were cyclically loaded or incrementally loaded to failure.

If the initial damage free stress state existing near the free edge uniquely influences the subsequent damage state and laminate strength then accurate out-of-plane elastic properties must be used when evaluating this stress state. To date only Dean and Turner [18], Ishikawa, Koyama, and Kobayashi [19], and Kriz and Stinchcomb [20] have obtained reasonable estimates of out-of-plane lamina properties. As pointed out by Crossman [14], out-of-plane properties used in most free edge stress analyses are rough approximations; therefore, only trends in stress fields can be demonstrated. In this investigation accurate wet, and dry out-of-plane elastic lamina properties will be used in various stress analysis methods to evaluate the wet and dry stress state both near and away from the free edge.

II. EXPERIMENTAL PROCEDURE

2.1 Environmental Conditioning

The specimens listed in Table 1 were fabricated by Southwest Research Institute and McDonnell Douglas using the same recommended procedure for curing Narmco T300/5208. Half of the specimens were exposed to 95% RH at 70°C, and the remaining specimens were dried in a dry nitrogen gas oven at 65°C. Although vacuum ovens have been commonly used for moisture desorption at elevated temperatures, damage is minimized when dry nitrogen gas is used [21]. Moisture absorbed or lost was measured as a change in weight. All specimens labeled as "WET" were in a condition of maximum absorbed moisture which occurred when no additional increase in specimen weight could be measured. All specimens labeled as "DRY" were in a condition of total absence of diffused moisture which was obtained when no additional loss in specimen weight could be measured.

2.2 Unidirectional Tension Tests

Both wet and dry $[0_8]$ and $[90_8]$ specimens listed in Table 1 were loaded to failure in tension using an Instron load frame with a crosshead speed of 0.1 inches per minute. Biaxial strains were measured at the center of each specimen using Micro-Measurement WA-00-120WT-350 strain gages. Young's moduli and Poisson's ratios were determined.

Static strengths were obtained for both $[0_8]$ and $[90_8]$ specimens in the wet and dry conditions. However, a series of strengths were obtained from each $[90_8]$ specimen. This was accomplished by testing

TABLE 1. SPECIMENS TESTED

Item No., (Specimen No.)	Quantity	Length (Inches)	Laminate Configuration Env. Condition	Test Type
M38(1-6)	6	12.0	$[0_8]$/Dry	Unidirectional Tension Test
M38(28-33)	6	12.0	$[0_8]$/Wet	Unidirectional Tension Test
M39(1-6)	6	12.0	$[90_8]$/Dry	Unidirectional Tension Test (Weakest Link)
M39(16-12)	6	12.0	$[90_8]$/Wet	Unidirectional Tension Test (Weakest Link)
S11*	1	7.0	$[0/\pm45/90]_s$/Dry	Preliminary Quasi-Isotropic Tension Tests
S12*	1	7.0	$[0/\pm45/90]_s$/Wet	Preliminary Quasi-Isotropic Tension Tests
S21*	1	7.0	$[0/90/\pm45]_s$/Dry	Preliminary Quasi-Isotropic Tension Tests
S22*	1	7.0	$[0/90/\pm45]_s$/Wet	Preliminary Quasi-Isotropic Tension Tests
M40(4-7,12-21, 34,35,36)	17	5.0	$[0/\pm45/90]_s$/Dry	Quasi-Isotropic Static Tension Tests
M40(34*,35,36)	3	7.0	$[0/\pm45/90]_s$/Wet	Quasi-Isotropic Static Tension Tests
M40(4-7)*	4	7.0	$[0/\pm45/90]_s$/Dry	Quasi-Isotropic Fatigue Tests
M40(12-21)	10	7.0	$[0/\pm45/90]_s$/Dry	Quasi-Isotropic Fatigue Tests
M40(8-11,24-33, 37,38,40)	17	5.0	$[0/\pm45/90]_s$/Wet	Quasi-Isotropic Static Tension Tests
M40(37*,38,40)	3	7.0	$[0/\pm45/90]_s$/Wet	Quasi-Isotropic Static Tension Tests
M40(8-11)*	4	7.0	$[0/\pm45/90]_s$/Wet	Quasi-Isotropic Fatigue Tests
M40(24-33)	10	7.0	$[0/\pm45/90]_s$/Wet	Quasi-Isotropic Fatigue Tests

TABLE 1. SPECIMENS TESTED
(continued)

Item No., (Specimen No.)	Quantity	Length (Inches)	Laminate Configuration Env. Condition	Test Type
M41(1-4,9-18, 34,35,36)	17	5.0	$[0/90/\pm45]_S$/Dry	Quasi-Isotropic Static Tension Tests
M41(34*,38,40)	3	7.0	$[0/90/\pm45]_S$/Dry	Quasi-Isotropic Static Tension Tests
M41(1-4)*	4	7.0	$[0/90/\pm45]_S$/Dry	Quasi-Isotropic Fatigue Tests
M41(9-18)	10	7.0	$[0/90/\pm45]_S$/Dry	Quasi-Isotropic Fatigue Tests
M41(5-8,24-33, 37,38,40)	17	5.0	$[0/90/\pm45]_S$/Wet	Quasi-Isotropic Static Tension Tests
M41(37*,38,40)	3	7.0	$[0/90/\pm45]_S$/Wet	Quasi-Isotropic Static Tension Tests
M41(5-8)*	4	7.0	$[0/90/\pm45]_S$/Wet	Quasi-Isotropic Fatigue Tests
M41(24-33)	10	7.0	$[0/90/\pm45]_S$/Wet	Quasi-Isotropic Fatigue Tests

S and M indicate specimens manufactured at South West Research Institute and McDonnell Douglas, respectively

* indicates specimen polished for replicas to be taken during test

the remaining sections after each failure. Using a minimum specimen length requirement of 1.5 inches, up to eight values of tensile strength could be measured for each initially unbroken 12 inch long $[90_8]$ specimen. Testing the $[90_8]$ specimens in this manner allows the experimentalist to isolate the first or "weakest link" strength from the subsequently higher strength values. Correlation of lamina strength values with laminate crack spacing equilibrium models developed by Reifsnider [17] was the objective of the weakest link $[90_8]$ tests. Elastic modulus was measured for all $[90_8]$ tests using a biaxial strain gage unless the previous break location was at or near the strain gage.

2.3 Preliminary Tension Tests of Quasi-Isotropic Laminates

The objectives of these static tests are to initially isolate unique free edge damage states in type I and type II laminates and show how these unique damage states develop into the characteristic damage state (CDS) when the laminate load is increased. The replica technique as utilized by Stalnaker and Stinchcomb [13] is best suited for recording and observing damage which develops along the laminate free edge. By using the replica technique an image of damage from a polished laminate free edge can be imprinted onto a thin acetate strip while the load is held constant. The image of free edge damage is transferred onto the acetate strip under pressure by simultaneously wetting the polished laminate surface and surface of the acetate with acetone. By using this technique the development of damage can be recorded by taking replicas in increments of increasing load. One edge on each specimen was polished with 3 micron alumina oxide particles using a standard metallographic

polishing wheel with felt cloth.

The specimens used in the preliminary static tests listed in Table 2 were fabricated by Soutwest Research Institute. Each specimen was incrementally loaded in tension by a hydraulic-load controlled Tinius Olsen machine. The replica technique was used to record the damage state before and after the wet and dry conditioning as well as at the various static load levels listed in Table 2. The interpretation of damage imprinted on the replicas was used as a basis for improved test procedures used in the quasi-isotropic static tension tests listed in Table 3. Strains along the load axis were measured at the center of each specimen using Micro-Measurements CEA-13-062VW-120 strain gages. The failure strength and Young's modulus were recorded for each specimen which was incrementally loaded to failure.

2.4 Quasi-Isotropic Static Tension Tests

As shown in Table 3 the specimens were divided into two groups. The first group of specimens were quasi-statically loaded to failure with no replicas. The second group of specimens were incrementally loaded to failure with replicas taken at 100 lb. intervals. The objective of the quasi-statically loaded tests was to statistically demonstrate the differences in wet or dry laminate strengths for type I and type II laminates. As discussed in the introduction, the difference between type I and type II experimentally determined laminate strengths provides a basis for investigating how the free edge damage develops under load and influences the laminate strength. It follows that the objective of the second group of tests is to demonstrate how the

TABLE 2. PRELIMINARY QUASI-ISOTROPIC TENSION TESTS

Item No.	Length (Inches)	Laminate Configuration/ Env. Condition	Replica Load Level (lbs x 100)
S11	7.0	$[0/\pm45/90]_s$/Dry	(0,2,3,6,8,10,12,14,20,22,24,26,27)
S12	7.0	$[0/\pm45/90]_s$/Wet	(0,2,10,15,20)
S21	7.0	$[0/90/\pm45]_s$/Dry	(0,2,3,6,8,10,12,14,20,26,30,32)
S22	7.0	$[0/90/\pm45]_s$/Wet	(0,2,10,15,20,30,32,33)

S indicates specimens fabricated by Southwest Research Institute

TABLE 3. QUASI-ISOTROPIC STATIC TENSION TEST

Item No., (Specimen No.)	Quantity	Length (Inches)	Laminate Configuration Env. Condition	Replica Load Level (lbs x 100)
M40(4-7,12-21, 34,35,36)	17	5.0	$[0/\pm45/90]_S$/Dry	No Replicas; Load, Quasi-Static to Fracture
M40(35,36)	2	7.0	$[0/\pm45/90]_S$/Dry	No Replicas; Load, Quasi-Static to Fracture
M40(8-11,24-33, 37,38,40)	17	5.0	$[0/\pm45/90]_S$/Wet	No Replicas; Load, Quasi-Static to Fracture
M40(38,40)	2	7.0	$[0/\pm45/90]_S$/Wet	No Replicas; Load, Quasi-Static to Fracture
M41(1-4,9-18), 34,35,36)	17	5.0	$[0/90/\pm45]_S$/Dry	No Replicas; Load, Quasi-Static to Fracture
M41(35,36)	2	7.0	$[0/90/\pm45]_S$/Dry	No Replicas; Load, Quasi-Static to Fracture
M41(5-8,24-33, 37,38,40)	17	5.0	$[0/90/\pm45]_S$/Wet	No Replicas; Load, Quasi-Static to Fracture
M41(38,40)	2	7.0	$[0/90/\pm45]_S$/Wet	No Replicas; Load, Quasi-Static to Fracture
M40(34*)	1	7.0	$[0/\pm45/90]_S$/Dry	Replicas (0',0,1-10,12,14,16,18,20,22)†
M40(37*)	1	7.0	$[0/\pm45/90]_S$/Wet	Replicas (0',0,1-22,24,25,26)†
M41(34*)	1	7.0	$[0/90/\pm45]_S$/Dry	Replicas (0',0,1-20,22,23,24,26,28,30,32,24)†
M41(37*)	1	7.0	$[0/90/\pm45]_S$/Wet	Replicas (0',0,1-20,22,24,26,28,32,34)†

† indicates specimens are incrementally load to fracture
0' indicates replica taken prior to Env. Condition

NOTE: All other symbols defined in Table 1

damage in wet or dry quasi-isotropic laminates develop into the characteristic damage state (CDS) prior to fracture of the laminate. In order to characterize the development of damage, replicas at 100 lb. load increments were obtained for only one specimen which was conditioned into a wet or dry state of stress. The four specimens which were incrementally loaded to failure are instrumented with biaxial strain gages located at the center of each specimen.

2.5 Quasi-Isotropic Fatigue Tests

The objective of the fatigue tests is to characterize the development of damage in wet and dry quasi-isotropic laminates when cyclically loaded. As shown in Table 4, replicas were taken for two types of cyclic loads. The coaxing cyclic load when used with replicas implies that the experimentalist can interact with the fatigue test such that a unique state of damage could be isolated or "coaxed" out of the laminate. When the steady state cyclic load is used the experimentalist records the regular sequence of damage events on replicas and does not interact with the fatigue test. The remaining fatigue tests are not replicated, but form a sufficient data base for studying the overall laminate response (i.e. residual strength, stiffness change) when using either the coaxing or steady state cyclic loads. Initial Young's modulus is measured using a MTS clip-on extensometer while the specimen is being quasi-statically preloaded up to the maximum cyclic load. All tests were cycled at 10 Hertz on a load controlled MTS machine. For both coaxing and steady state cyclic loads the change in Young's moduli is periodically measured by stopping the test and reloading up to

TABLE 4. QUASI-ISOTROPIC FATIGUE TESTS

Item No., (Specimen No.)	Quantity	Length (Inches)	Laminate Configuration Env. Condition	Cyclic Load Type Load Level (ibs x 100)
M40(4*)	1	7.0	$[0/\pm45/90]_s$/Dry	Coaxing (0',0,Δ^2[16],10K,50K,100K)*
M40(5-7)*	3	7.0	$[0/\pm45/90]_s$/Dry	Steady State (0',0,Δ^2[20],5K,10K,50K,100K,1M)*
M40(12-20)	9	7.0	$[0/\pm45/90]_s$/Dry	Steady State (1[50],5K,10K,50K,100K)$\Delta E\%$
M40(21)	1	7.0	$[0/\pm45/90]_s$/Dry	Steady State (1[50],5K,10K,50K,100K)$\Delta E\%$
M40(8*)	1	7.0	$[0/\pm45/90]_s$/Wet	Coaxing (0',0,Δ^2[20],5K,10K,50K,100K)*
M40(10*)	1	7.0	$[0/\pm45/90]_s$/Wet	Steady State (0',0,Δ^2[20],5K,10K,50K,100K)*
M40(9,11)*	2	7.0	$[0/\pm45/90]_s$/Wet	Steady State (0',0,Δ^2[20],5K,10K,50K,100K,1M)*
M40(24-31,33)	9	7.0	$[0/\pm45/90]_s$/Wet	Steady State (1[50],5K,10K,50K,100K)$\Delta E\%$
M40(32)	1	7.0	$[0/\pm45/90]_s$/Wet	Steady State (1[50],5K,10K,50K,100K,1M)$\Delta E\%$
M41(1*)	1	7.0	$[0/90/\pm45]_s$/Dry	Coaxing (0',0,Δ^2[18],5K,10K, 50K,100K,1M,1.5M)*
M41(2,3)*	2	7.0	$[0/90/\pm45]_s$/Dry	Steady State (0',0,Δ^2[20],5K,10K,50K,100K)*
M41(4*)	1	7.0	$[0/90/\pm45]_s$/Dry	Steady State (0',0,Δ^2[20],5K,10K,50K,100K,1M)*
M41(9-17)	9	7.0	$[0/90/\pm45]_s$/Dry	Steady State (1[50],5K,10K,50K,100K)$\Delta E\%$
M41(18)	1	7.0	$[0/90/\pm45]_s$/Dry	Steady State (1[50],5K,10K,50K,100K,1M)$\Delta E\%$
M41(8*)	1	7.0	$[0/90/\pm45]_s$/Wet	Coaxing (0',0,Δ^2[12],2.5M,2.6M,2.7M)*
M41(5,7)*	2	7.0	$[0/90/\pm45]_s$/Wet	Steady State (0',0,Δ^2[20],5K,10K,50K,100K)*
M41(6*)	1	7.0	$[0/90/\pm45]_s$/Wet	Steady State (0',0,Δ^2[20],5K,10K,50K,100K,1M)*
M41(24-32)	9	7.0	$[0/90/\pm45]_s$/Wet	Steady State (1[50],5K,10K,50K,100K)$\Delta E\%$
M41(33)	1	7.0	$[0/90/\pm45]_s$/Wet	Steady State (1[50],5K,10K,50K,100K,1M)$\Delta E\%$

TABLE 4. QUASI-ISOTROPIC FATIGUE TESTS
(continued)

0'	indicates replicas taken before wet or dry Environmental Conditioning
Δ^2[...]	indicates 200 lb load increments up to max. load (lbs x 100) as indicated in brackets
1[...]	indicates quasi-static preload up to max. stress (ksi) as indicated in brackets
ΔE%	indicates only a change in modulus recorded at load levels or cycles
*	indicates replicas and modulus recorded at load level or cycles indicated in paranthesis
K	indicates a thousand cycles
M	indicates a million cycles

the maximum cyclic load. A constant stress ratio of 0.1 was used for all fatigue tests. The drying out of all wet specimens during the fatigue tests was eliminated by simply wrapping a wet paper towel around the test specimen.

In order to coax the desired unique free-edge damage state the experimentalist should be able to stop the test momentarily and observe the development of damage. The author discovered that the image of damage replicated onto an acetate strip can be immediately viewed on a microfiche card reader with sufficient magnification and clarity for interpretation. The experimentalist can then interpret the state of damage during the test and decide which test variables should be changed in order to further isolate or alter the observed damage. As a result of this interactive test technique, no clearly defined test procedure is established. Although the test procedure is open ended, the experimentalist must base his interpretation of damage on a rational mechanistic approach. This requires an understanding of the initial damage free stress state and the CDS which will be explained in Chapter III. Therefore the guidelines or rationale used to interpret the damage state when using the coaxing cyclic load is outlined in Section 4.4.1 following Chapter III. One specimen from each wet and dry stress state was fatigued by a coaxing cyclic load. Replicas at 200 lb. intervals and residual strengths were obtained by incrementally loading the specimens to failure.

The objective of the steady state cyclic load tests is to record the regular sequence of damage events which develop into the

characteristic damage state. Replicas are taken at 200 lb. intervals during the initial preload up to the maximum loads listed in Table 4. Replicas were also taken at 5K, 10K, 50K, and 100K cycles. For each wet and dry stress state, two specimens were cycled to 100K cycles and one specimen cycled to 1M cycles. Residual strengths were obtained after 100K or 1M cycles with replicas taken at 100 lb. intervals.

III. STRESS ANALYSIS

3.1 Linear Elastic Homogeneous Transversely Isotropic (LEHTI) Material Properties

For fiber-reinforced composite laminates it has been experimentally demonstrated [13] that damage initiates near the laminate free edge in the form of ply cracking and interply delaminations. Finite element and finite difference models and perturbation solutions [34,24,25] were developed in order to predict stresses near the free edge prior to the formation of damage. Both the finite element and finite difference models require all nine orthotropic lamina properties. If the initial damage-free stress state existing near the free edge uniquely influences the subsequent formation of damage then accurate out-of-plane elastic properties (e.g. ν_{23} and G_{23}) must be used when evaluating this stress state. Unfortunately all nine elastic lamina properties are difficult to obtain; therefore it is not uncommon to make simplifying approximations, such as $\nu_{23}=\nu_{12}=\nu_{13}$ and $G_{23}=G_{12}=G_{13}$, in order to obtain solutions. A parametric evaluation by Kriz [26] of these approximations and other property variations on the interlaminar stresses in angle-ply laminates demonstrates that more emphasis should be placed on accurately calculating or experimentally measuring all lamina elastic properties if meaningful stress distributions are to be obtained from the various models.

In this investigation each laminate layer (lamina) is assumed to be constructed of fiber reinforced materials as shown in Figure 1. When the fibrous lamina are assumed to be homogeneous and transversely isotropic, the number of independent material constants reduces to

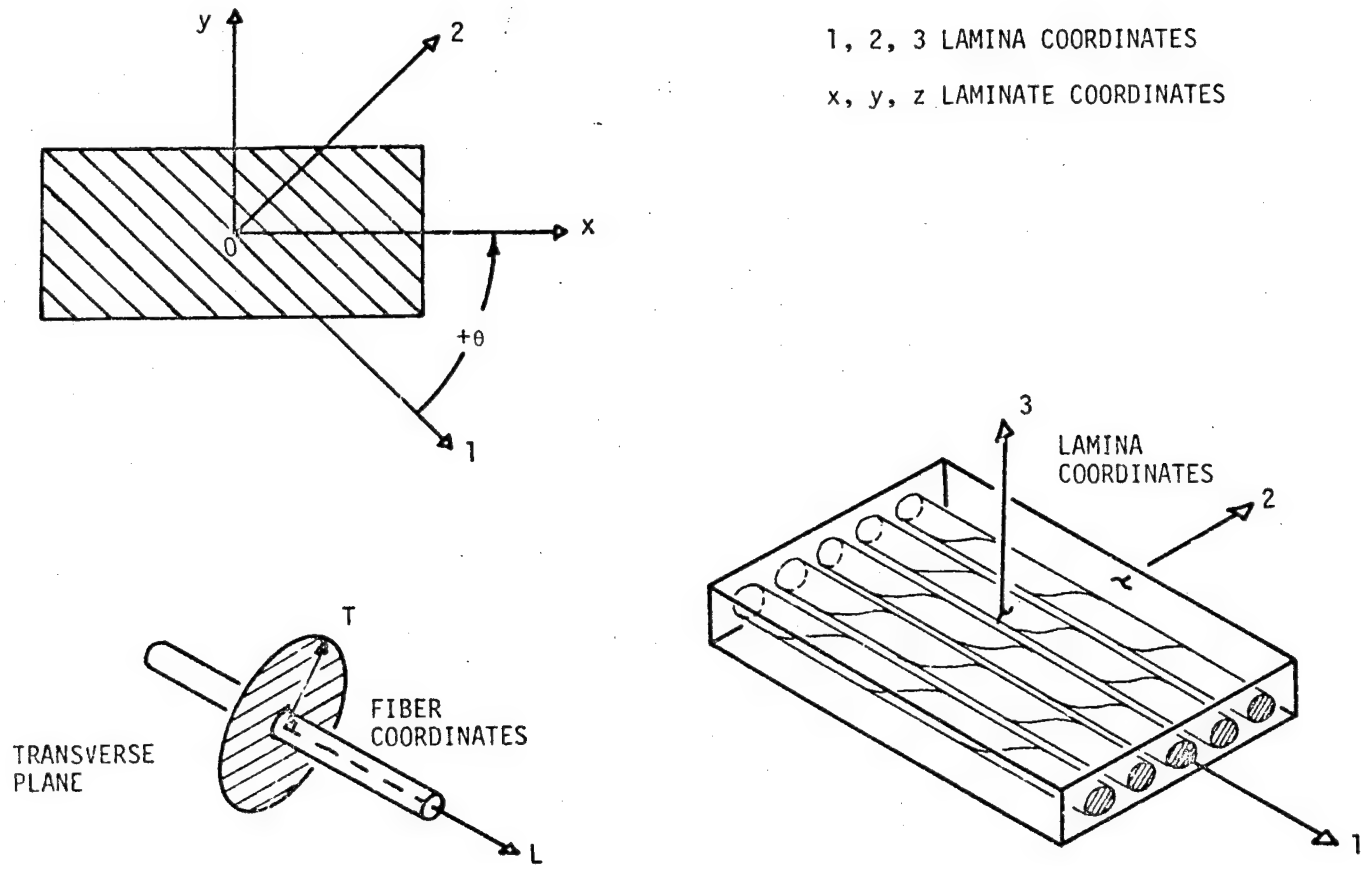

FIGURE 1. COORDINATE SYSTEM DEFINITION

five. The most commonly used engineering constants are listed below:

$$E_1,\ E_2 = E_3,\ G_{12} = G_{13},\ \nu_{12} = \nu_{13},\ G_{23}$$

The symbols, E, G, and ν are Young's modulus, shear modulus, and Poisson's ratio, respectively, and numbered subscripts refer to the lamina coordinates, shown in Figure 1. For transversely isotropic materials, the Poisson's ratio in the 2-3 plane is related to E_2 and G_{23} by Equation (1)

$$\nu_{23} = E_2/2G_{23}-1 \qquad (1)$$

Reasonable estimates for ν_{23} and G_{23} together with other laminate elastic properties have been obtained experimentally using mechanical and ultrasonic techniques [18,19,20]. A complete set of elastic lamina properties, including ν_{23} and G_{23}, can be calculated using equations developed by Hashin [27] as listed in Appendix B given the isotropic matrix and transversely isotropic fiber elastic properties. Unfortunately the complete set of transversely isotropic graphite fiber properties are difficult to obtain due to the small fiber diameter.

Dean and Turner [18] demonstrated that most of the graphite fiber properties could be determined by curve fitting ultrasonically evaluated stiffnesses over a range of fiber volume fraction by using Hashin's equations written in terms of ultrasonic stiffnesses. Unfortunately, due to scatter in ultrasonic data, Dean and Turner were unable to extrapolate for all fiber properties. Kriz and Stinchcomb [20] improved on the extrapolation technique of Dean and

Turner and showed that although ultrasonic data are scattered, all fiber properties can be determined and that five independently extrapolated graphite fiber properties are consistent with the assumption that fibers can be modeled as transversely isotropic. However, there is an error in the equations used by Kriz and Stinchcomb [20] to calculate values of G_{23}. The correct expression for β_2 is shown below in Equation (2) where β_2 is used in Equation B.2(b) of Appendix B to calculate G_{23}. Fortunately all graphite/epoxy

$$\beta_2 = \frac{K_{f_{tt}}}{K_{f_{tt}} + 2G_{f_{tt}}} \qquad (2)$$

lamina properties which depend on the correction for β_2 are changed by less than 1 percent. It is also noted that the corrections have no effect on the extrapolated fiber properties. Therefore, all observations and conclusions by Kriz and Stinchcomb [20] are unaltered. Although these corrections are not numerically significant for the graphite/epoxy materials evaluated in Ref. [20], there could be other fiber/matrix systems for which these corrections could become significant.

Graphite/epoxy lamina properties were also experimentally measured by Ishikawa et al [19] using mechanical test techniques and fiber properties were extrapolated. Comparison of extrapolated graphite fiber properties along with epoxy matrix properties is demonstrated in Table 5. A final set of fiber and matrix elastic properties are chosen and listed in Table 6.

Since fibers properties are assumed unchanged by moisture,

TABLE 5. SUMMARY OF GRAPHITE FIBER AND EPOXY MATRIX ELASTIC PROPERTIES

Reference No.	Experimental Method Used to Determine Elastic Properties	Matrix Properties				Matrix Material
		E_m (Msi)	G_m (Msi)	ν_m	K_m (Msi)	
-	Ultrasonic	0.836	0.306	0.368[c]	1.16[c]	5208[1]
20	Ultrasonic	0.766[e]	0.283[e]	0.353[e]	0.963[e]	LY556
19	Mechanical	0.498	0.180	0.380	0.750[c]	Epikote 828[3]
22	Ultrasonic	0.573	0.212	0.355	0.658[c]	DER 322[4]

Reference No.	Experimental Method Used to Determine Elastic Properties	Fiber Properties						Fiber Material
		E_{fL} (Msi)	G_{fLT} (Msi)	G_{fTT} (Msi)	ν_{fLT}	ν_{fTT}	K_{fTT} (Msi)	
20	Ultrasonic	33.7[e]	3.48[e]	0.728[e]	0.29[e]	0.49[e]	2.17[e]	Modmore II[2]
19	Mechanical	32.4[e]	6.68[e]	0.950[e]	0.30[c]	0.42[e]	2.93[e]	T300 A[3]

1 Narmco Brand Name
2 Rolls Royce LTD
3 TORAY Industries, Inc., Japan
4 Dow Chemical Branch Name
c indicates value calculated from experimental data
e indicates value extrapolated from experimental data

TABLE 6. WET AND DRY ELASTIC PROPERTIES

Type	Material	Elastic Properties Dry/Wet (% Difference)					
Matrix	5208 Epoxy	E_m(Msi)		G_m (Msi)		ν_m	
		0.776/0.575 (-25%)		0.283/0.207 (-27%)		0.353/0.388 (+10%)	
Fiber	T300 Graphite	E_{fL} (Msi)	G_{flT} (Msi)	G_{fTT} (Msi)	ν_{fLT}	ν_{fTT}	E_{fT} (Msi)
		33.71 -	3.481 -	0.7281 -	0.2901 -	0.4901 -	2.171 -
Lamina	T300/5208 Graphite/ Epoxy v_f=0.55%	E_1 (Msi)	G_{12} (Msi)	G_{23} (Msi)	ν_{12}	ν_{23}	E_2 (Msi)
		18.9/18.8 (-0.5%)	0.782/0.603 (-23%)	0.472/0.410 (-13%)	0.308/0.323 (+4.6%)	0.492/0.323 (+8.1%)	1.41/1.26 (-11%)
Laminate	T300/5208 $[0/\pm45/90]_s$ $[0/90/\pm45]_s$	E_x, Calculated from Laminate Theory using Lamina Properties					
		7.41/7.18 (-3.1%)					
Shear Transfer Layer	T300/5208 v_f-0.42%	G_{SL}, Dry Property obtained from Reference [16]					
		0.650/0.488 (-25%)					

the wet/dry lamina properties listed in Table 6 are calculated by substituting the fiber properties together with the wet/dry matrix properties into the equations listed in Appendix B. The changes in elastic matrix properties due to moisture absorbtion are chosen such that the corresponding changes in elastic lamina properties, reflect experimental differences in wet/dry lamina properties. For example, an 11 percent reduction in lamina modulus, E_2, is calculated when a 25 percent decrease in matrix modulus, E_m, together with a 27 percent reduction in matrix shear modulus, G_m, are substituted into the equations of Appendix B. The predicted decrease of 11 percent for E_2 is comparable with experimental reductions of 10.7 percent by Hahn [28] and 11.2 percent by Hofer et al [29]. A decrease of 0.5 percent is predicted for E_1 which does not compare well with a decrease of 4.5 percent measured by Hahn and Kim [28] and 16.3 percent measured by Hofer [29]. An insufficient data base on wet/dry T300/5208 lamina shear properties does not provide meaningful comparison with the predicted reductions of 23 percent for G_{12} and 13 percent for G_{23}. To date no reliable and reproducible shear test method has been widely accepted to verify the trends predicted for G_{12} and G_{23}.

Variations in test techniques together with variations in test specimens due to manufacturing processes, quality control, etc. are obvious problems which account for much of the variation in experimental data. Variations in fiber volume fraction, temperature and duration of cure [22] could provide additional explanations for variations in experimental data. For these reasons the author has choosen to select

lamina properties as calculated from the equations in Appendix B which model the change in experimental data due to moisture absorption as a reduction of matrix elastic properties. The experimental value of 18.8 Msi was chosen for E_1 corresponding to a fiber volume fraction of 55 percent as calculated from equations in Appendix B when fiber and wet matrix properties were chosen. Wet and dry type I and type II laminate stiffnesses were calculated from laminate plate theory using the wet and dry lamina properties at 55 percent fiber volume fraction. To be consistent with previous analysis [16] a value of 0.65 msi was chosen for the shear transfer layer modulus, G_{SL}. Interestingly, a value of 0.65 msi is calculated for G_{12} when at a fiber volume fraction of 42 percent is used in Equation (13) of Appendix B. It is reasonable to assume that the shear transfer which acts over a small distance above and below a resin rich interface should have a slightly lower fiber volume fraction when compared to 55 percent in the plies adjacent to the interface.

The fiber, matrix, lamina, laminate, and interface elastic properties were chosen to demonstrate how variations in wet and dry conditioning of type I and type II laminates affect the free edge stresses and subsequent development of damage at the free edge. Variations in experimentally measured elastic lamina properties can be large. For this reason the lamina elastic properties were chosen such that only variations due to moisture absorption are modeled using the equations of Appendix B. Elastic properties chosen in this way do not include the inherent variations in experimentally

measured elastic properties. These properties provide a consistent set of elastic properties to be used in the 2-D, 3-D, and crack spacing models following this section.

3.2 Two Dimensional Thin Laminate Theory Stress State

The first approximation of a laminate stress state, neglecting out-of-plane stresses (plane stress is assumed), is obtained by laminated plate theory. Since the laminate thickness is much smaller than its other dimensions Kirchhoff's hypothesis can be used. As a result of these approximations each layer of the laminate is assumed to be in a state of plane stress which can be directly related to inplane loads and moments. A complete development of the classical thin laminated plate theory is given by Jones [30]. The objective of this section is to predict the stresses existing in the thin laminate plane prior to the damage event, using laminate theory, and assuming no initial damage exists. The predicted stresses are the result of an applied in-plane mechanical load acting together with residual stresses due to swelling from moisture absorption and curing at elevated temperatures.

The combined effect of a mechanical load, N_x, and residual stresses, σ_i^R, on the individual ply stresses, σ_i, is shown in Equation (3) using the notation of Kim and Hahn [11].

$$\sigma_i = Q_{ij} A_{jk}^{-1} N_k + \sigma_i^R \qquad (3)$$

where

Q_{ij} = reduced ply stiffnesses

A_{ij} = laminate stiffnesses

N_k = laminate stress resultants

σ_i^R = residual ply stresses

The residual ply stresses, σ_i^R, can be represented in terms of differences in lamina and laminate thermal and moisture strains.

$$\sigma_i^R = Q_{ij}(\varepsilon_j^{oT} - \varepsilon_j^T) + Q_{ij}(\varepsilon_j^{oM} - \varepsilon_j^M) \tag{4}$$

where

ε_j^{oT} = laminate thermal strain

ε_j^{oM} = laminate moisture strain

ε_j^T = lamina thermal strain

ε_j^M = lamina moisture strain

These strains can be defined in terms of coefficients of expansion.

$$\sigma_i^R = Q_{ij}(\bar{\alpha}_j - \alpha_j)\Delta T + Q_{ij}(\bar{\beta}_j - \beta_j)\Delta M \tag{5}$$

where

α_j = lamina thermal coefficient of expansion

β_j = lamina moisture coefficient of expansion

ΔT = change in temperature

ΔM = percent weight gained by moisture absorption

$\bar{\alpha}_j$ = laminate thermal coefficient of expansion

$\bar{\beta}_j$ = laminate moisture coefficient of expansion

Laminate coefficients of expansion are defined by integrating the lamina strains written in terms of coefficients of expansion through the laminate thickness, (-h/2, h/2), as shown below.

$$\bar{\alpha}_i \equiv A^{-1}_{im} \int_{-h/2}^{h/2} Q_{mn}\alpha_n dz \tag{6}$$

$$\bar{\beta}_i \equiv A^{-1}_{im} \int_{-h/2}^{h/2} Q_{mn}\beta_n dz \tag{7}$$

For the type I and type II laminates, damage first occurs in the 90° plies in the form of cracks transverse to the direction of the uniaxial laminate tension load, N_x. Since cracks first occur in the 90° plies we calculate the stresses in this ply by expanding equation (3), as shown below,

$$\sigma_1 = \frac{Q_{12}Q_{yy}-Q_{11}A_{xy}}{A_{xx}A_{yy}-A^2_{xy}} N_x + \sigma^R_1 \tag{8}$$

$$\sigma_2 = \frac{Q_{22}A_{yy}-Q_{12}A_{xy}}{A_{xx}A_{yy}-A^2_{xy}} N_x + \sigma^R_2 \tag{9}$$

$$\sigma_6 = 0 \tag{10}$$

where subscripts 1 and 2 refer to the lamina coordinates defined in Figure 1 and subscript 6 is the contracted notation for the lamina shear stress in the 1-2 plane. The initial crack in the 90° ply is labeled FPF for first ply failure and the corresponding laminate load is labeled, N_x^{FPF}. Although σ_1 and σ_2 both exist in the 90° ply at FPF the transverse stress, σ_2, has reached the transverse strength while σ_1 is much lower than the longitudinal strength. Therefore a maximum stress failure criterion can be used which assumes FPF occurs when the

value of σ_2 in equation (9) is equal to the unconstrained uniaxial tensile strength, T, of a 90° test specimen. Using the maximum stress failure criterion, equation (9), can be used to solve for N_x^{FPF} by replacing σ_2 with T.

$$N_x^{FPF} = \frac{A_{xx}A_{yy}-A_{xy}^2}{Q_{22}A_{yy}-Q_{12}A_{xy}} (T-\sigma_2^R) \tag{11}$$

Prediction of the FPF laminate load, N_x^{FPF}, depends on how accurately σ_2^R is predicted. From equation (5) the value calculated for σ_2^R depends upon approximations made for lamina thermal and moisture coefficients together with realistic estimates of percent weight gained due to moisture absorption, ΔM, and changes in temperature, ΔT, from the stress free temperature. By measuring the warpage of unsymmetric [±θ] laminates Pagano and Hahn [31] suggest a stress free cure temperature of 250°F for T300/5208 which is considerably lower than the 350°F cure temperature. For T300/5208 graphite/epoxy Hahn [28] measured lamina thermal and moisture coefficients of expansion, as shown below.

$$\alpha_1 = -0.17\ \mu\varepsilon/°F;\ \alpha_2 = 15.6\ \mu\varepsilon/°F,\ \beta_1 \equiv 0;\ \beta_2 = 5900\ \mu\varepsilon/\%H_2O \tag{12}$$

where β_2 is calculated from experimental data assuming a moisture threshold, C_v, of 0.4% as shown in Figure 2. Independently Crossman [10] demonstrated that swelling of T300/5208 graphite/epoxy exhibits the same moisture threshold with less scatter of data and measured lamina thermal and moisture coefficients of expansion shown below.

$$\alpha_1 = 0.16\ \mu\varepsilon/°F;\ \alpha_2 = 14.3\ \mu\varepsilon/°F;\ \beta_1 \equiv 0;\ \beta_2 = 5000\ \mu\varepsilon/\%H_2O \tag{13}$$

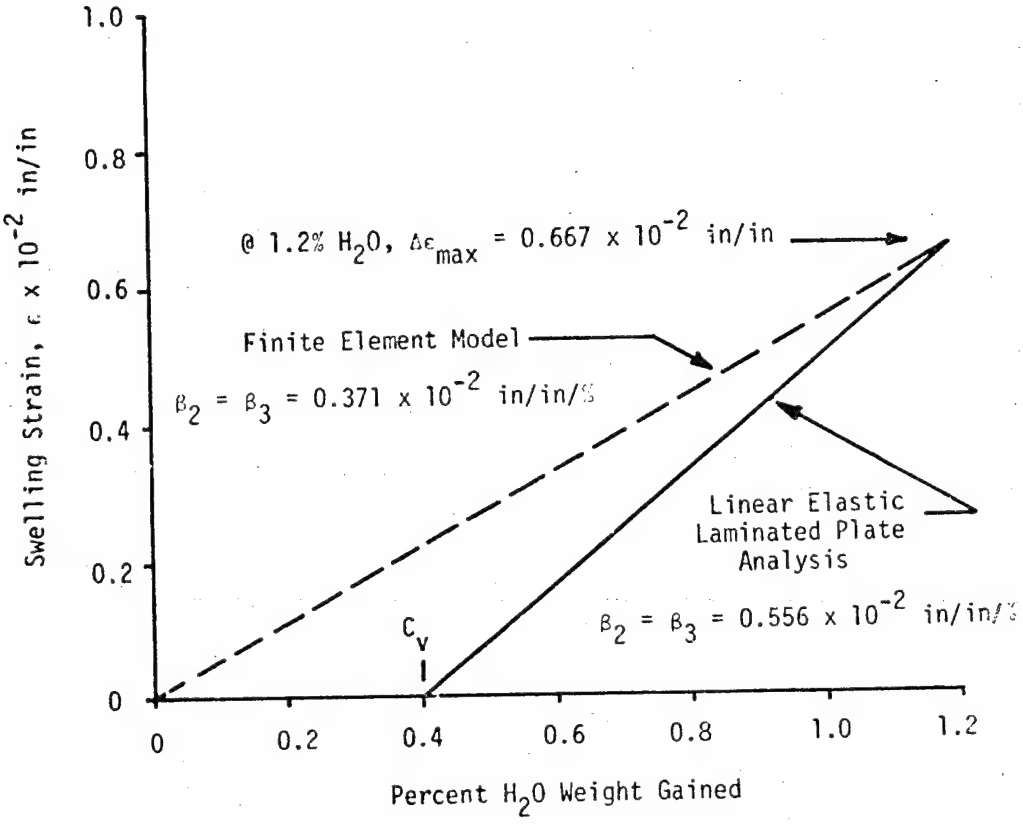

FIGURE 2. MOISTURE COEFFICIENT OF EXPANSION APPROXIMATION

The coefficients of thermal expansion shown below were the same as used by Nagarkar and Herakovich [32] and moisture expansion coefficients were obtained by curve fitting experimental data reported by Crossman [10] assuming a moisture threshold of 0.4%.

$$\alpha_1 = -0.23\ \mu\varepsilon/°F;\ \alpha_2 = 14.9\ \mu\varepsilon/°F;\ \beta_1 \equiv 0;\ \beta_2 = 5560\ \mu\varepsilon/\%H_2O \tag{14}$$

The laminate thermal and moisture coefficients of expansion are calculated for type I and type II laminates by substituting the wet and dry elastic properties listed in Table 6 together with the lamina expansion coefficients (14) into equations (6) and (7).

$$\bar{\alpha}_{XDRY} = \bar{\alpha}_{YDRY} = 1.09\ \mu\varepsilon/°F;\ \bar{\beta}_{XDRY} = \bar{\beta}_{XDRY} = 484\ \mu\varepsilon/\%H_2O$$

$$\bar{\alpha}_{XWET} = \bar{\alpha}_{YWET} = 0.98\ \mu\varepsilon/°F;\ \bar{\beta}_{XWET} = \bar{\beta}_{YWET} = 444\ \mu\varepsilon/\%H_2O$$

It is now possible to calculate wet and dry residual stresses at room temperature by using equation (5) where ΔM was measured as 1.2 percent in the fully saturated state and a temperature change of -180°F was estimated using Hahn's approximation of 250°F for the stress free temperature. The Q_{ij} were calculated using wet and dry properties listed in Table 6.

$$\sigma^R_{2DRY} = 3.43\ \text{ksi} \qquad \sigma^R_{2WET} = -1.96\ \text{ksi} \tag{15}$$

The laminate FPF load is now calculated from equation (9) using elastic properties in Table 6 together with the difference between the transverse strength, T, and the residual stress state. The values for

the weakest or first transverse strengths, T, as described in Section 2.2 are listed in Table 10 and used in Equation (11) to calculate N_X^{FPF}. Using only dry properties in equation (11), a dry FPF laminate load, N_{XDRY}^{FPF}, was calculated. Similarly a wet FPF laminate load, N_{XWET}^{FPF}, was calculated using only wet properties.

$$N_{XDRY}^{FPF} = 789 \text{ lb/in} \qquad N_{XWET}^{FPF} = 1900 \text{ lb/in} \tag{16}$$

The FPF laminate loads for type I and type II laminates, predicted by laminate theory, are identical since changing the stacking sequence has no effect on σ_2^R.

It is interesting to note that the predicted wet residual stress state σ_{2WET}^R in the 90° ply is in compression by -1.96 ksi. For this reason a higher laminate load is required to produce FPF when the laminate has absorbed 1.2 percent moisture by weight gain.

Although this section was primarily concerned with evaluating the stress state in the 90° ply prior to FPF, all 0° and 45° ply stresses in the wet or dry state have also been calculated using equation (3) in similar fashion. The calculated ply stresses for N_{XDRY}^{FPF} and N_{XWET}^{FPF} are listed in Tables 7 and 8 for comparison with the predicted finite element stresses in Section 3.3 which use the same wet and dry FPF laminate loads.

3.3 Three Dimensional Finite Element Theory (LEHTI) Stress State

The objective of this section is to predict, using finite element theory, the stresses existing in the interior and along the edge of type I and type II laminates prior to the first damage event. The

TABLE 7. SUMMARY OF INTERIOR AND EDGE σ_x, σ_y, AND σ_z STRESSES FOR WET OR DRY QUASI-ISOTROPIC TYPE I AND TYPE II LAMINATES

Model Type	Laminate Configuration	M, Midplane I, Interface (Ply Angle)	(Dry Interior Stress/Dry Edge Stress)(Wet Interior Stress/Wet Edge Stress)(ksi)		
			σ_x	σ_y	σ_z
LELPA	$[0/+45/90]_s$	M(0°)	(+41.3/ -)(113.0/ -)	(+3.44/ -)(-1.91/ -)	0
		M(45°)	(+11.2/ -)(+25.8/ -)	(+6.35/ -)(+16.4/ -)	0
		M(-45°)	(+11.2/ -)(+25.8/ -)	(+6.35/ -)(+16.4/ -)	0
		M(90°)	(+6.47/ -)(+4.74/ -)	(-16.1/ -)(-30.8/ -)	0
FEM	$[0/+45/90]_s$	M(0°)	(+41.5/+40.5)(113.0/113.0)	(+3.23/+0.07)(-2.10/-0.28)	(0 /0.05)(0 /-1.37)
		I			
		M(45°)	(+11.2/+6.90)(+25.8/+9.32)	(+6.35/+0.05)(+16.4/-0.10)	(0 /+3.92)(0 /-2.41)
		I			
		M(-45°)	(+11.2/+7.28)(+25.8/+9.21)	(+6.35/+0.37)(+16.4/+0.22)	(0 /+3.54)(0 /+4.38)
		I			
		M(90°)	(+6.27/+9.22)(+4.56/+9.27)	(-15.9/-0.14)(-30.8/-0.37)	(0 /+5.25)(0 /+7.03)
LELPA	$[0/90/+45]_s$	M(0°)	(+41.3/ -)(113.0/ -)	(-3.44/ -)(-1.91/ -)	0
		M(90°)	(+6.47/ -)(+4.74/ -)	(-16.1/ -)(-30.8/ -)	0
		M(45°)	(+11.2/ -)(+25.8/ -)	(+6.35/ -)(+16.4/ -)	0
		M(-45°)	(+11.2/ -)(+25.8/ -)	(+6.35/ -)(+16.4/ -)	0
FEM	$[0/90/+45]_s$	M(0°)	(+41.5/+40.6)(113.0/113.0)	(+3.23/+0.43)(-2.10/+0.10)	(0 /+2.01)(0 /+1.02)
		I			
		M(90°)	(+6.26/+8.04)(+4.55/+6.12)	(-15.9/-0.25)(-30.8/-0.50)	(0 /+2.87)(0 /+1.71)
		I			
		M(45°)	(+11.2/+6.46)(+25.8/+7.80)	(+6.34/+0.32)(+16.4/-0.06)	(0 /+1.18)(0 /-0.48)
		I			
		M(-45°)	(+11.2/+5.92)(+25.8/+6.79)	(+6.34/+0.03)(+16.4/-0.25)	(0 /-2.22)(0 /-6.44)

TABLE 8. SUMMARY OF INTERIOR AND EDGE τ_{yz}, τ_{xz}, AND τ_{xy} STRESSES FOR WET OR DRY QUASI-ISOTROPIC TYPE I AND TYPE II LAMINATES

Model Type	Laminate Configuration	M, Midplane I, Interface (Ply Angle)	(Dry Interior Stress/Dry Edge Stress)(Wet Interior Stress/Wet Edge Stress)(ksi)		
			τ_{yz}	τ_{xz}	τ_{xy}
LELPA	$[0/\pm45/90]_s$	M(0°) M(45°) M(-45°) M(90°)	0 0 0 0	0 0 0 0	(0 / -)(0 / -) (+3.81/ -)(+19.7/ -) (-3.81/ -)(-19.7/ -) (0 / -)(0 / -)
FEM	$[0/\pm45/90]_s$	M(0°) I M(45°) I M(-45°) I M(90°)	(0 /-3.39)(0 /+1.47) (0 /-0.22)(0 /-0.57) (0 /-2.77)(0 /-4.21) (0 /-0.01)(0 /-0.05)	(0 /-0.26)(0 /+1.52) (0 /-0.08)(0 /-8.59) (0 /+0.03)(0 /+1.34) (0 /+0.01)(0 /+0.06)	(0 /+0.07)(0 /-0.44) (+4.02/+0.02)(+19.9/+1.58) (-4.02/+0.09)(-19.9/-1.53) (0 /+0.05)(0 /+0.37)
LELPA	$[0/90/\pm45]_s$	M(0°) M(90°) M(45°) M(-45°)	0 0 0 0	0 0 0 0	(0 / -)(0 / -) (0 / -)(0 / -) (+3.81/ -)(+19.7/ -) (-3.81/ -)(-19.7/ -)
FEM	$[0/90/\pm45]_s$	M(0°) I M(90°) I M(45°) I M(-45°)	(0 /-2.19)(0 /-0.64) (0 /+0.19)(0 /-0.26) (0 /+2.70)(0 /+3.43) (0 /+0.33)(0 /+0.50)	(0 /+0.11)(0 /+0.48) (0 /+0.20)(0 /+0.97) (0 /+0.21)(0 /+1.81) (0 /-0.61)(0 /-9.22)	(0 /+0.02)(0 /-0.09) (0 /-0.06)(0 /-0.37) (+4.01/+0.04)(0 /-0.37) (-4.01/-0.09)(-19.9/-1.51)

predicted stresses are the result of a wet or dry FPF laminate load, which were calculated in section 3.2, acting together with residual stresses due to swelling from moisture absorption and shrinking after cooling down from an elevated stress free temperature.

The Finite Element Model (FEM) used in this section was developed at Virginia Tech in the Engineering Science and Mechanics Department by graduate students under the direction of Dr. Carl Herakovich. Several thesis and dissertations [32,33,34,35] have been involved in the development of this FEM. The current version of the FEM (NONCOM III) was used in this investigation. The general formulation of this FEM is reported in the most recent reference [32].

The FEM represents the laminate in a state of generalized plane strain in the x load direction by using constant strain triangles as shown in Figure 3. Because of symmetry conditions for type I and type II laminates only a quarter of the y-z plane is modeled. Boundary conditions are imposed such that all nodes along $y = 0$ are constrained from moving in the y-direction but are free to move in the z-direction, and all nodes along $z = 0$ are constrained from moving in the z-direction but are free to move in the y-direction. The common node at $y = 0$, $z = 0$ is held fixed. The externally applied nodal forces along $Z = H$ and $y = B$ are prescribed to be zero. These prescribed nodal forces represent the free edge and free surface stress-free boundary conditions. The FEM grid used to model the four layer quarter plane as shown in Figure 3 uses 768 elements and 438 nodes with 96 triangular elements at the laminate edge. As

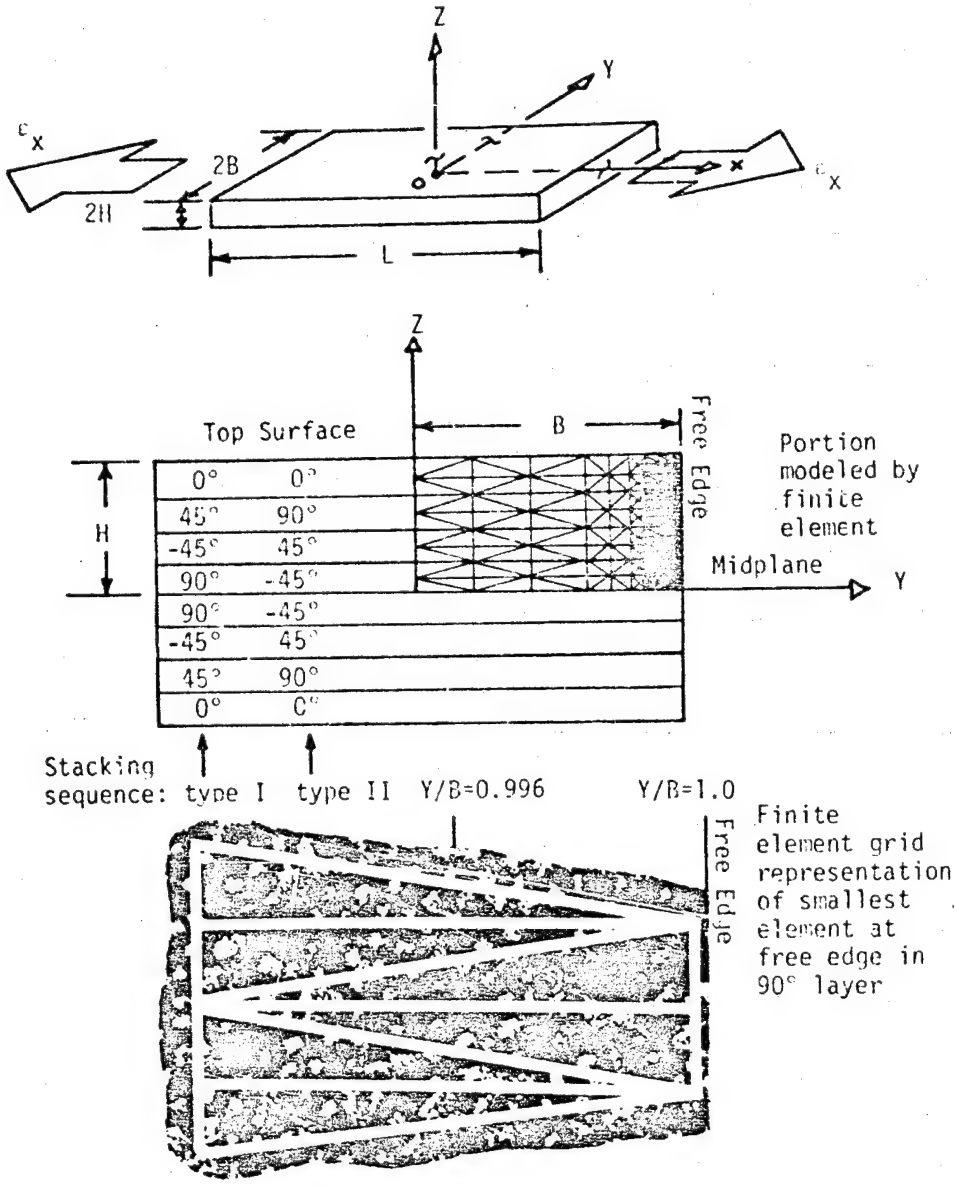

FIGURE 3. LAMINATE GEOMETRY AND FINITE ELEMENT GRID REPRESENTATION

shown in Figure 3 the size of the elements are reduced near the free edge in order to model the stress gradients in this region. The smallest edge element used in this dissertation is shown in Figure 3 such that 15-20 fibers fill the triangular area with at least 3 fibers along the triangular edge.

Although the finite element method is not limited by how small the elements are chosen, the smallest element was chosen, in this investigation, such that the composite material modeled within the smallest element shown in Figure 3 can be assumed to behave as a homogeneous material. This is only a limitation on the idealization of homogeneity used in the constitutive relations by the finite element method.

The author chose not to model the nonlinearities of T300/5208 since Crossman [10] experimentally verified that the calculated linear elastic residual stress state can be used as an approximation for predicting the curvature of unsymmetric T300/5208 laminates. Although the differences between the experimental and predicted curvatures are most likely due to nonlinearities of T300/5208, these differences are small and are ignored in order to minimize the number of approximations introduced into an idealized FEM. The point is made that these nonlinearities are not insignificant, but that there is much yet to be explained about FPF, as will be demonstrated in Section 4.5, when using only the linear elastic idealization. A case in point is the crack spacing model developed by Reifsnider et al [16] which uses an idealized linear elastic shear lag model to predict the crack spacing following the FPF event.

Only the linear elastic facility of the FEM (NONCOM III) is utilized by using the wet and dry elastic properties listed in Table 6 together with the lamina expansion coefficients (14) from section 3.2 where $\Delta T = -180°F$ and $\Delta M = 1.2$ percent. Since the present FEM is not formulated with respect to Hahn's moisture threshold, c_v, the β_2 expansion coefficient is recalculated to give the same maximum swelling strain as shown in Figure 2. For comparison with the FPF stress state calculated in section 3.2, the same wet and dry FPF laminate loads are used by the FEM to predict the edge stress state. In order to study the combined effect of the moisture, temperature, and FPF laminate load on the edge stresses, the FEM calculates the edge stresses due to moisture, temperature, and FPF load separately and then superposes the stresses to idealize the final wet and dry edge stress state for type I and type II laminates.

Although it may be instructive to demonstrate how the initial residual dry stresses changes with stacking sequence, followed by moisture absorption and mechanical load, only the final superposed wet or dry edge and interior stress states existing prior to damage formation are presented in the section. Crossman [10,14] has already provided an interesting evaluation on how various stacking sequences, uniformily distributed moisture levels and applied loads affect the edge stress state. The emphasis in the present investigation is to compare the final superposed wet or dry edge and interior stress states existing prior to damage formation with the first formation of damage as observed using the replica technique.

The free edge and interior stress state for a type I wet laminate with a wet FPF laminate load is graphically demonstrated in Figures 4-11. A four element averaging scheme outlined in reference [35] is used to calculate average σ_z, τ_{xz}, and τ_{yz} stress distributions along the laminate interfaces as shown in Figures 4-6. The same four element averaging scheme is used to average σ_x, σ_y, and τ_{xy} stresses along the midlayers as shown in Figures 7-9. Through the thickness distributions plotted in Figures 10 and 11 use a two element averaging scheme.

Only stress distributions for type I wet are shown in Figures 4-11. The edge and interior values of stress for the type I dry, type II dry and type II wet laminates are summarized in Tables 7 and 8 along with the laminate plate theory stress state for comparison. As a check all interior FEM stresses are equivalent to stresses predicted by laminate theory, as shown in Tables 7 and 8. Minor variations in the interior stresses between FEM and laminate theory exist since laminate theory models the σ_x, σ_y, and τ_{xy} stresses as constants within the layer with a discontinuity in stress between layers.

For later reference with respect to formation of edge damage, the damage free σ_x and σ_z stress state for wet and dry type I and type II laminates are compared in Figure 12.

3.4 Characteristic Damage State Model Definition

The characteristic damage state (CDS) was first introducted by Reifsnider et al [16] as a laminate property which could be defined

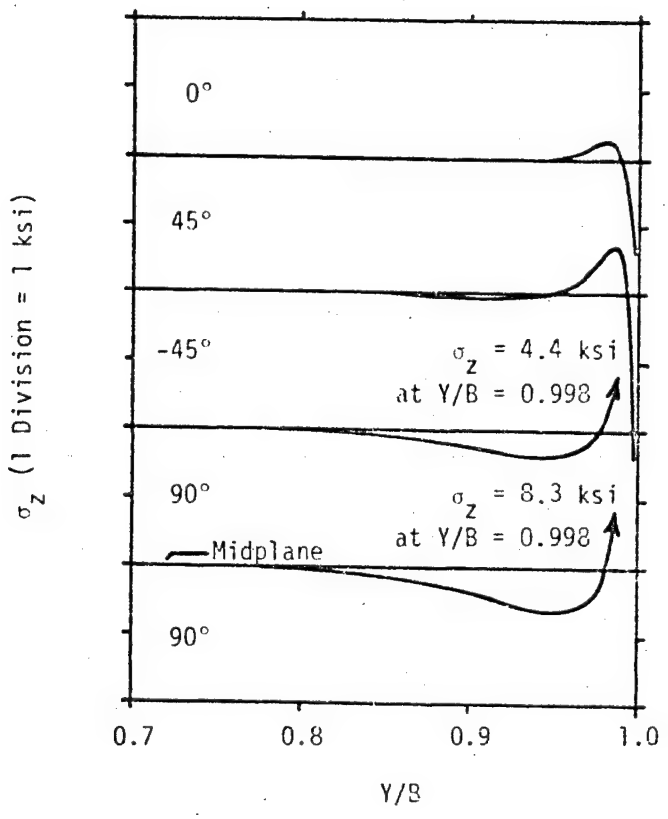

FIGURE 4. VARIATION OF σ_z NEAR THE FREE EDGE OF A TYPE I WET LAMINATE (N_x=1900 lb/in, ΔT=-180°F, ΔM=1.2%)

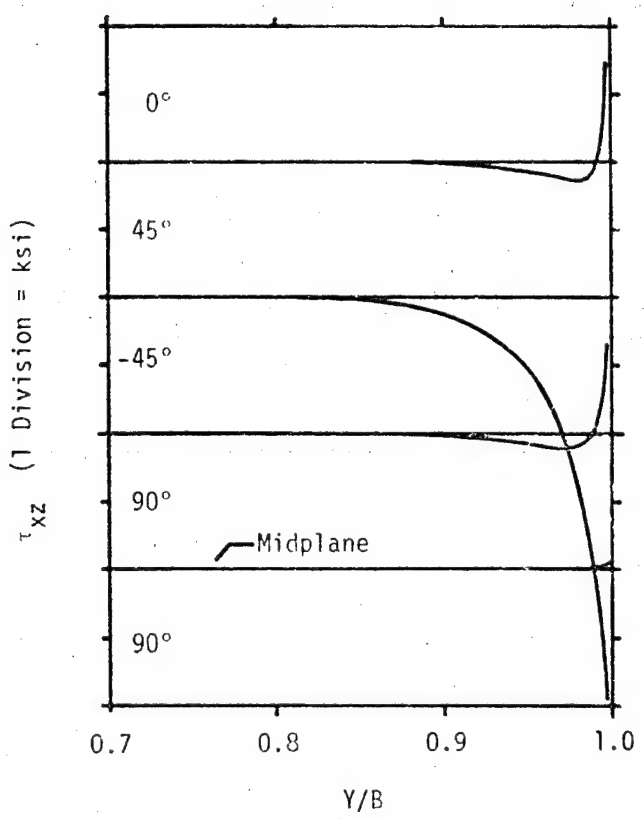

FIGURE 5. VARIATION OF τ_{xz} NEAR THE FREE EDGE OF A TYPE I WET LAMINATE (N_x=1900 lb/in, ΔT=-180°F, ΔM=1.2%)

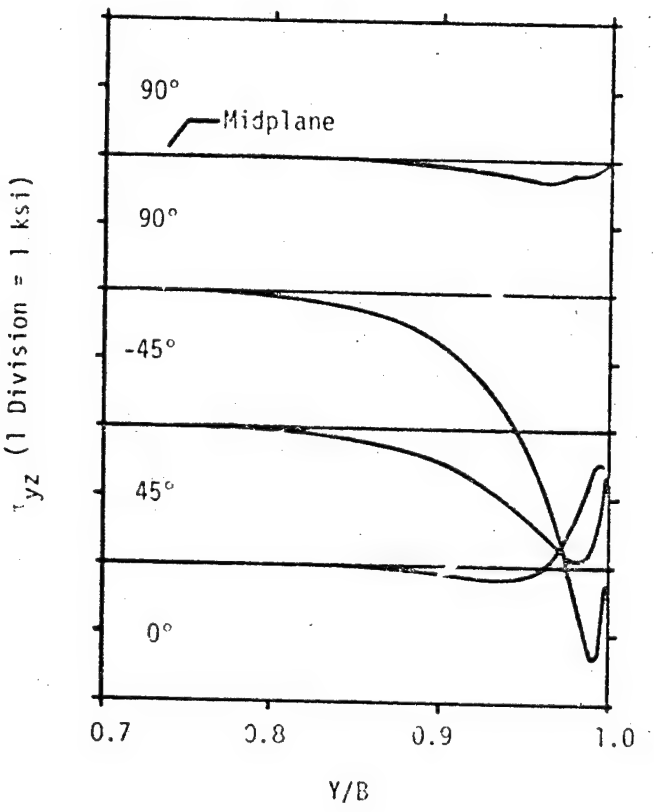

FIGURE 6. VARIATION OF τ_{yz} NEAR THE FREE EDGE OF A TYPE I WET LAMINATE (N_x=1900 lb/in, ΔT=-180°F, ΔM=1.2%)

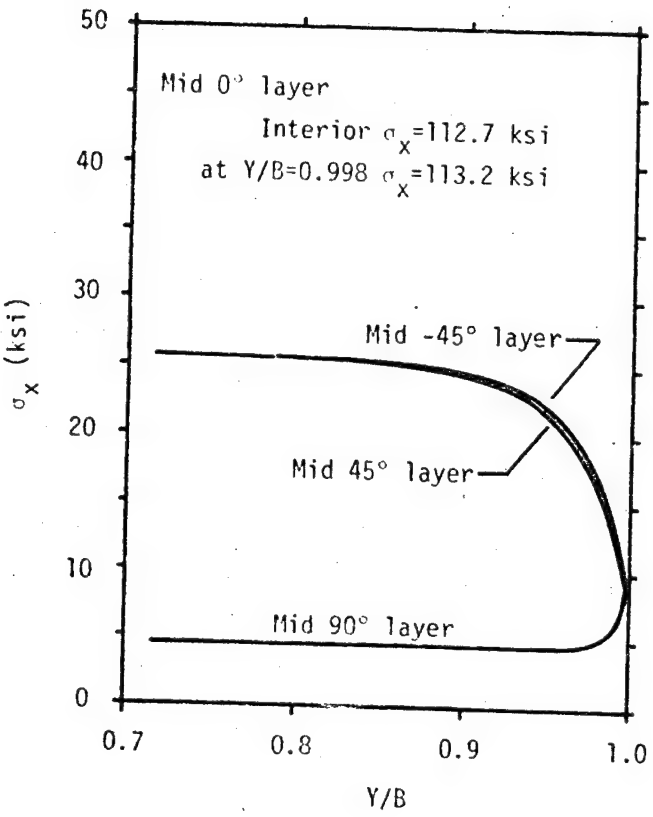

FIGURE 7. VARIATION OF σ_x NEAR THE FREE EDGE OF A TYPE I WET LAMINATE (N_x=1900 lb/in, ΔT=-180°F, ΔM=1.2%)

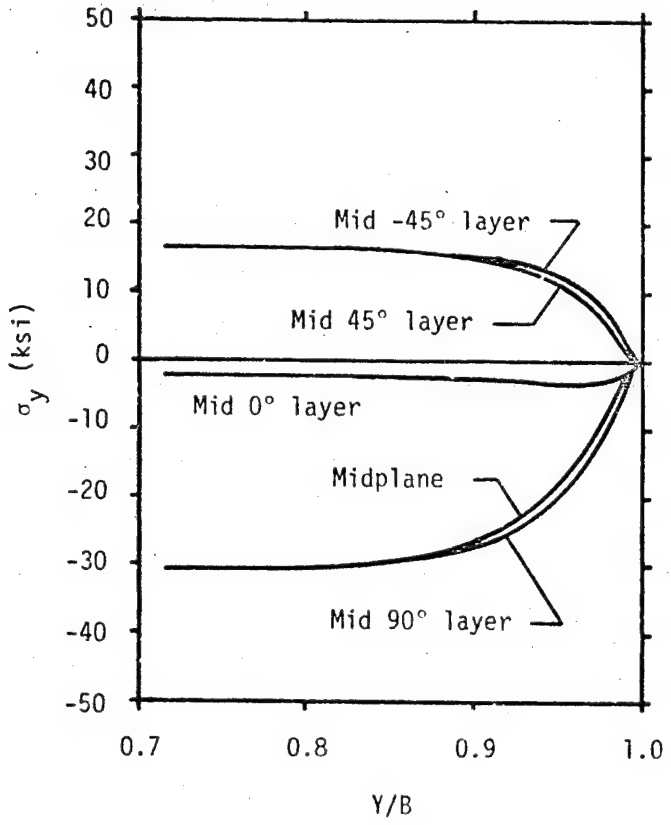

FIGURE 8. VARIATIONS OF σ_y NEAR THE FREE EDGE OF A TYPE I WET LAMINATE (N_x=1900 lb/in, ΔT=-180°F, ΔM=1.2%)

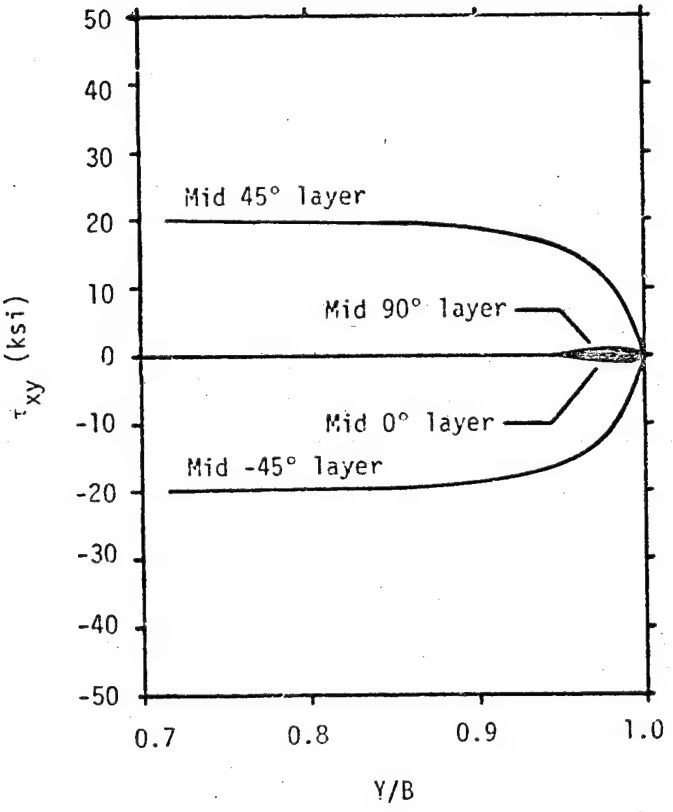

FIGURE 9. VARIATION OF τ_{xy} NEAR THE FREE EDGE OF A TYPE I WET LAMINATE (N_x=1900 lb/in, ΔT=-180°F, ΔM=1.2%)

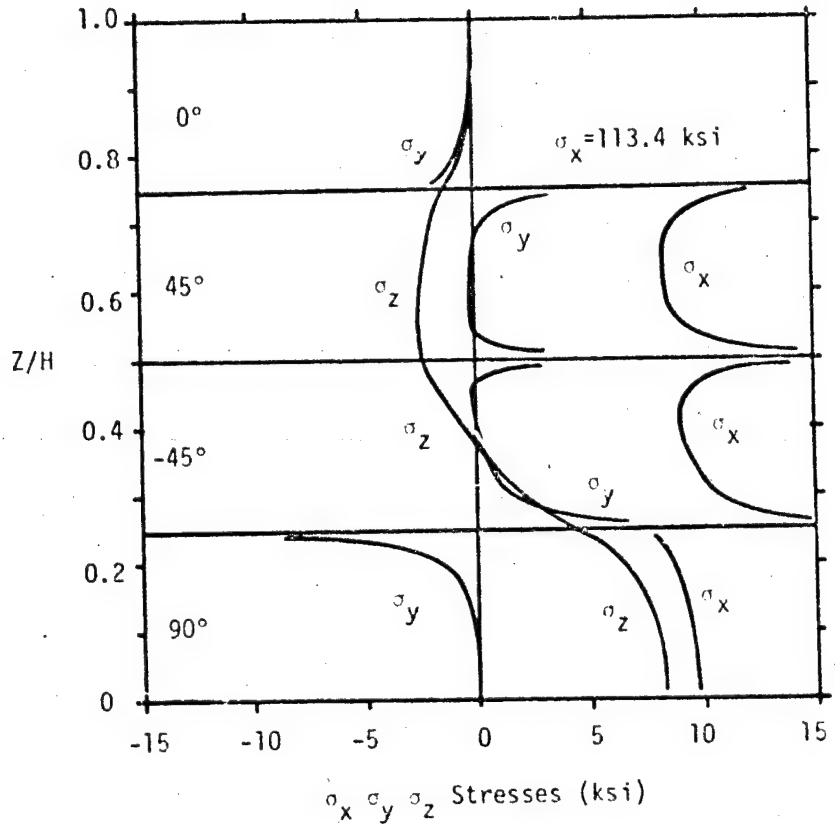

FIGURE 10. VARIATION OF σ_x σ_y AND σ_z THROUGH THE THICKNESS AT Y/B=0.998 FOR A TYPE I WET LAMINATE (N_x=1900 lb/in, ΔT=-180°F, ΔM=1.2%)

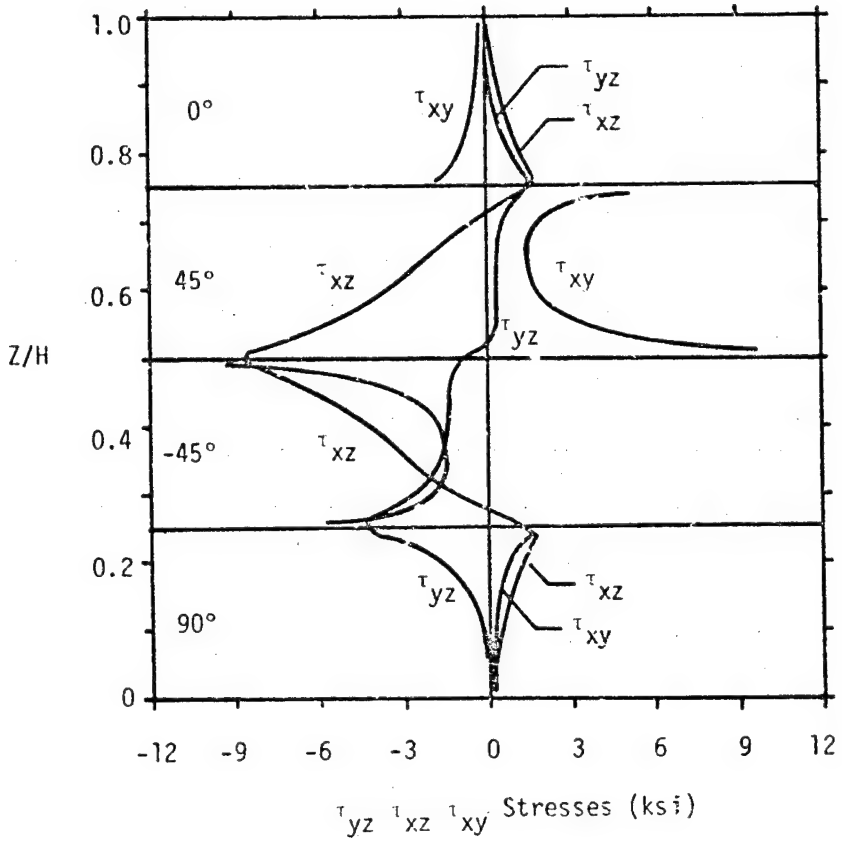

FIGURE 11. VARIATION OF τ_{yz}, τ_{xz}, τ_{xy} THROUGH THE THICKNESS AT Y/B=0.998 FOR A TYPE I WET LAMINATE (N_x=1900 lb/in, ΔT=-180°F, ΔM=1.2%)

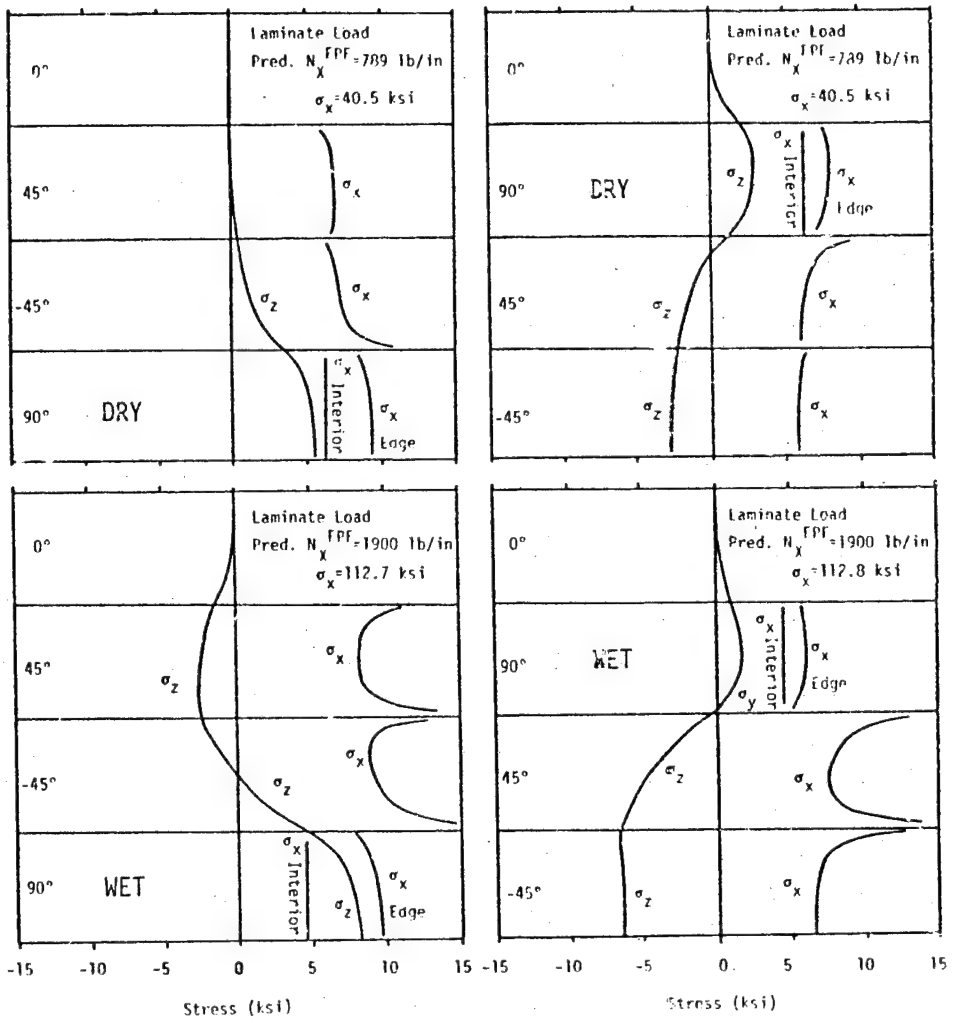

FIGURE 12. COMPARISON OF σ_x AND σ_z FPF STRESSES IN WET AND DRY TYPE I AND TYPE II LAMINATES AT Y/B=0.998

as a predictable and regular pattern of ply cracks which exists prior to fracture. Definition of the damage state prior to fracture is facilitated by a shear lag model, employed in reference [16], in order to predict the stable patterns of ply cracks which develop after the FPF event. Although other damage in the form of interply cracks and longitudinal ply cracks exists, the stable pattern of ply cracks form the basis of the CDS. Understanding how this crack pattern and subsequent stresses are distributed in this CDS prior to fracture should explain the difference in fracture strengths for type I and type II laminates. Talug [36] investigated the states of stress surrounding a partially damaged region in type I and type II laminates and demonstrated the differences that exist in the response of these laminates even in regions remote from the edges.

The shear lag model developed in references [37,38] predict crack spacing in 90° plies with increasing load. This shear lag model was developed for the specific case where the plies adjacent to the 90° plies are of the same orientation. Since this restriction prohibits the use of these models for a type II laminate, where the 90° plies are constrianed by 0° and 45° plies, the more general shear lag model formulated by Reifsnider et al [16] is used in this investigation. The concept of a characteristic crack pattern which is introduced by Reifsnider et al [16] is also utilized in this investigation.

Although much work is being done to further characterize how the CDS uniquely influences the laminate response, the effort in this investigation is to better define the CDS with respect to the effect of

moisture. Since the stable pattern of cracks is the basis of the CDS, the effects of moisture on the crack patterns will be demonstrated. The shear lag model is developed by Reifsnider et al [16] in sufficient detail such that only basic principles are restated below.

The shear lag model assumes that when a FPF crack forms in an off axis ply the σ_x stress in the ply is recovered from zero at the crack surface to the unbroken ply stress as shown in Figure 13. The stress near the FPF is no longer carried through the cracked ply but is transfered by shear through plies adjacent to the cracked ply until the stress in the cracked ply has recovered to 99.9 percent of the unbroken stress which results in the formation of a second crack. The distance between the first and second crack is referred to as the crack spacing. Cracks continue to form in this manner with increasing laminate load until no new cracks form at which point an equilibrium crack spacing is reached. Ideally the cracked ply carries only 99.9% of the unbroken stress until equilibrium crack spacing is realized and then the cracked ply no longer carries any stress. The crack spacing is said to be characteristic of the laminate since ply and laminate elastic properties are used together with the ply strength to calculate distance between cracks. The effect of the stacking sequence on the crack spacing is included in the shear lag model by the constraining effect of adjacent plies on the redistribution of stress near the crack.

For type I laminates the redistribution of stress in the crack ply due to a shear transfer is formulated by Reifsnider et al [16]

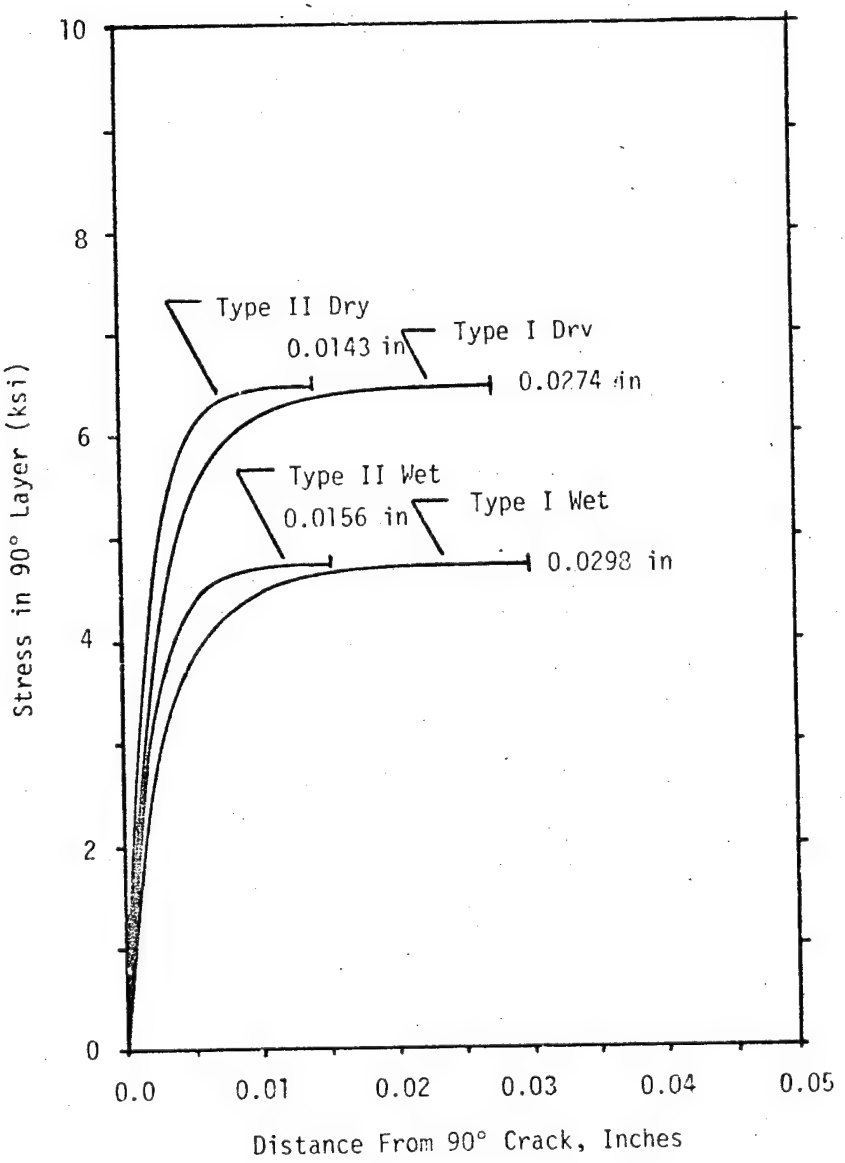

FIGURE 13. INFLUENCE OF WET AND DRY ELASTIC PROPERTIES ON THE PREDICTED CRACKING SPACING IN TYPE I AND TYPE II QUASI-ISOTROPIC LAMINATES

in more general terms by using normalized displacement, u, where the governing differential equations shown below are the result of an equilibrium element analysis analogous to the approach used in references [39,40].

$$A \frac{d^2 u_{90}}{dx^2} + u_{45} - u_{90} = 0 \tag{17}$$

$$B \frac{d^2 u_{45}}{dx^2} + u_{90} + x - 2u_{45} = 0 \tag{18}$$

Boundary conditions

$$\frac{du_{90}}{dx} (x \to \infty) = 1 \tag{19}$$

$$\frac{du_{45}}{dx} (x \to \infty) = 1 \tag{20}$$

$$\frac{du_{90}}{dx} (x = 0) = 0 \tag{21}$$

$$u_{45} (x = 0) = 0 \tag{22}$$

where

$$A = (b\ E_{90})/(2a\ E_x) \tag{23}$$

$$B = (b\ c\ E_{45})/(a^2\ E_x) \tag{24}$$

$$U = [\sigma_z a/\sqrt{E_x G_{SL}}]u \tag{25}$$

$$X = \sqrt{E_x/G_{SL}}\ a\ x \tag{26}$$

x = normalized distance from crack surface

u_{90} = normalized displacement in 90° ply

u_{45} = normalized displacement in 45° ply

U = displacement

X = distance

σ_z = stress applied to laminate

E_x = laminate stiffness

E_{90} = 90° ply stiffness

G_{SL} = shear transfer layer shear modulus

a = 90° ply thickness

b = shear transfer layer thickness

c = 45° ply thickness

Solutions to the differential equations are given below,

$$u_{90} = x + c_1 e^{-\alpha x} + c_2 e^{-\beta x} \tag{27}$$

$$u_{45} = x + D_1 c_1 e^{-\alpha x} + D_2 c_2 e^{-\beta x} \tag{28}$$

where

$$\alpha,\beta = \left[\frac{B+2A}{2AB} \pm \frac{1}{2AB}\left(B^2 + 4A^2\right)^{1/2}\right]^{1/2} \tag{29}$$

$$D_1 = 1 - A\alpha^2 \tag{30}$$

$$c_1 = -D_2/(\beta D_1 - \alpha D_2) \tag{31}$$

$$D_2 = 1 - A\beta^2 \tag{32}$$

$$c_2 = D_1/(\beta D_1 - \alpha D_2) \tag{33}$$

A similar set of solutions for the displacements in the type II laminate can be calculated from a different set of differential equations given in reference [16] but are too lengthy to be listed here along with the general solutions.

It can now be shown how moisture affects the crack spacing as defined in this section.

3.5 Influence of Environmental Conditioning on CDS

The influence of environmental conditioning on the CDS for type I and type II laminates is demonstrated in this section by showing how absorbed moisture changes the predicted crack spacing of the CDS as defined in section 3.4.

The crack spacing is characteristic of the laminate since the constraining effect of the stacking sequence is used together with the ply and laminate properties to calculate the distance between cracks. Although the shear lag model can be conveniently explained in terms of shear stress transfer of adjacent plies and the redistribution of stress, the shear lag model is more general when formulated in terms of normalized displacement, u. Stresses existing in a cracked ply are unique to the material type whereas solutions of the shear lag model, when calculated in terms of normalized displacement, are more general and can be applied to any material type. For these reasons it is more general to define the distance between cracks in terms of the normalized distance, x, when the normalized strain, du/dx, reaches a value of 0.999. Since the crack spacing is more generally defined in terms of normalized strain, du/dx, and distance, x, it follows from

the formulation in section 3.4 that the effect of moisture absorption on x, when du/dx is equal to 0.999, can only be accounted for by a reduction in ply and laminate elastic properties. A wet and dry distance, x, at du/dx = 0.999 is calculated using wet and dry elastic properties, respectively, as listed in Table 6. A decrease of 0.4 percent is calculated for the normalized distance, x, between cracks when 1.2 percent moisture is absorbed. When the normalized distance, x, is renormalized by using equation (26), the differences in wet and dry distance, X, between cracks, as shown in Figure 13 is increased by a net 9 percent. The redistribution of stresses plotted in Figure 13 is calculated by differentiating equation (25) with respect to X and multiplying the resulting strain by E_{90} such that the undisturbed stress in the cracked ply which has recovered 99.9 percent of its value is equated to the ply strength. As a result of these calculations, variations in the ply strength due to wet or dry conditioning have no effect on the predicted crack spacing model described in section 3.4. The net increase in crack spacing due to moisture absorption is mainly due to the factor $\sqrt{E_x/G_{SL}}$ as shown in Equation (26) since the resin rich shear transfer layer modulus, G_{SL}, is reduced more by moisture than is the laminate modulus, E_x. Predicted crack spacing for wet and dry type I and type II laminates is summarized in Table 9.

As a final note, the residual stress state in no way affects the rate of recovery of the stress from the crack to the undisturbed value of the ply stress (ply strength). The compressive wet residual 90° ply stress, σ^R_{2WET}, calculated in section 3.2, results in a higher

TABLE 9. SUMMARY OF PREDICTED AND EXPERIMENTAL CRACK SPACING IN 90° PLIES OF TYPE I AND TYPE II QUASI-ISOTROPIC LAMINATES

Test Type	Laminate Configuration/ Env. Condition	Laminate Load (lb/in)	Experimental/Predicted 90° Ply Equil. Crack Spacing (Inches)
Preliminary	$[0/\pm45/90/\mp45/0]_T$/dry	2000*	0.0145/ -
	$[0/\pm45/90/\mp45/0]_T$/wet	2000	0.0259/ -
Preliminary	$[0/90/\pm45]_S$/dry	3200	0.0113/ -
	$[0/90/\pm45]_S$/wet	3200	0.0251/ -
Static	$[0/\pm45/90]_S$/dry	1200*	0.0278/0.0274
	$[0/\pm45/90]_S$/wet	1700*	0.0627/0.0298
Static	$[0/90/\pm45]_S$/dry	1400*	0.0128/0.0143
	$[0/90/\pm45]_S$/wet	3000*	0.0130/0.0156

*Indicates load corresponds to equilibrium crack spacing.

laminate load to initiate FPF even though the transverse strength is reduced by moisture absorption. After the residual wet compressive stress has been eliminated by the laminate tension load followed by FPF the stress recovery from the cracked surface is unaffected by any previous residual stress state. As a result, the distance between cracks is unaffected by residual stress states.

The predicted FPF laminate loads and crack spacing discussed in this section and previous sections can now be compared with respect to the damage at the laminate edge which is recorded using the replica technique discussed in section 2.3.

IV. DISCUSSION OF EXPERIMENTAL RESULTS

4.1 Results of Environmental Conditioning

As discussed in section 2.1 all specimens listed in Table 1 were either dried until all diffused moisture was desorbed (Dry) or exposed to a 95% RH at 70°C until the maximum amount of diffused moisture was absorbed (Wet). Replicas of specimens designated with asterisks in Table 1 were taken before and after environmental conditioning. No damage was observed on replicas as a result of environmental conditioning. Initial damage prior to environmental conditioning was observed only for specimens 41 (3,4) as four transverse cracks in the center -45° plies of the type II laminates. When specimens 41 (3,4) were dried as previously described no additional damage resulted from the desorption.

Before continuing with the discussion of damage events in the following sections, a clarification should be made on interpretation of damage as observed on replicas. The laminate edge damage when transferred onto the acetate strip is assumed to be negligibly influenced by the acetone due to the short time of exposure. Seven succesive replicas were taken while the laminate load was held constant at a value greater than N_x^{FPF} and no additional damage was observed to have occurred due to possible weakening of material at the free edge surface during the exposure to acetone. The image of edge damage as transferred onto the acetate is not as clearly seen when compared to image of edge damage when directly viewed through a

microscope. For this reason the enlargement of a replica from the surface of fiber ends in a 90° ply was used in Figure 3 to demonstrate the loss of resolution. A trade off is made between quickly recording edge damage for later observation as opposed to a more time consuming but more detailed microscopic observation. Kim and Hahn [11] successfully used acoustic emissions (AE) to record damage in the form of FPF but AE is limited in this respect. The experimenter must ascertain whether the resolution of damage as transferred onto an acetate strip has sufficient clarity to demonstrate the damage of interest. In this effort only damage in the form of cracks, one ply thickness in length is of interest. Any cracks smaller than this are not considered to have eventful influences on the damage as defined by the CDS. As discussed in the introduction, cracks most likely originate at the fiber matrix interface; but until the cracks grow to the size of a ply thickness the cracks smaller than a ply thickness will have no effect on the CDS, as defined in section 3.4.

4.2 Results of Unidirectional Tests

The wet and dry $[0_8]$ and $[90_8]$ specimens listed in Table 1 were loaded to failure as described in section 2.2. Young's moduli for both types of specimens, in the wet and dry conditions are listed in Figure 15. Wet and dry strengths for both types of specimens are listed in Figure 14, and compared graphically with other lamina and laminate strengths in Figure 16. The wet and dry weakest link strengths for the $[90_8]$ specimens are listed in Table 10. The

Data Description	Mat'l Condition		Average Strength ± Stand. Dev. (Msi)
$[0,\pm45,90]_s$ Type I Static Tensile Strength	Ref. (14) Dry		
	Dry		72.8 ± 3.8
	Wet		76.2 ± 4.2
$[0,90,\pm45]_s$ Type II Static Tensile Strength	Wet		83.9 ± 4.4
	Dry		85.5 ± 3.5
	Ref. (14) Dry		
Type I Residual Strength 100K Cycles	Dry		72.3 ± 3.3
	Wet		69.2 ± 4.0
Type II Residual Strength 100K Cycles	Wet		80.4 ± 5.0
	Dry		80.4 ± 4.9
$[0_8]$ Static Tensile Strengths	Dry		213 ± 26.0
	Wet		206 ± 21.0
$[90_8]$ Weakest Link Static Tensile Strengths	DRY	1	6.47 ± 0.79
		2	7.34 ± 0.64
		3	7.65 ± 0.60
		4	7.92 ± 0.68
		5	7.68 ± 0.36
		6	7.39 ± 0.10
		7	8.17 -
		8	7.13 -
	WET	Break No.	
		1	4.74 ± 1.02
		2	4.98 ± 0.48
		3	4.70 ± 0.71
		4	5.14 ± 0.79
		5	4.66 ± 0.58
		6	5.13 ± 0.75
		7	5.03 ± 0.87
		8	5.46 ± 0.66
		9	5.32 -

FIGURE 14. SUMMARY OF STRENGTH DATA

Data Description	Mat'l Condition		Average Modulus ± Stand. Dev. (msi)	
Modulus $[0_8]$	Dry		21.2 ± 0.74	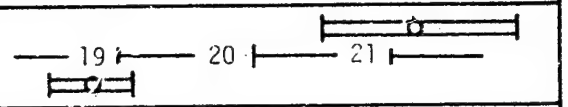
	Wet		18.8 ± 0.30	
Modulus $[90_8]$	Dry		1.60 ± 0.26	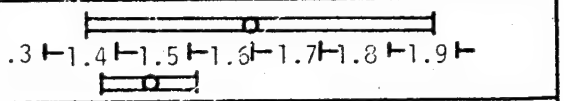
	Wet		1.45 ± 0.07	
Modulus Type I Quasi-static load Rate=20 lb/sec	Dry		7.39 ± 0.16	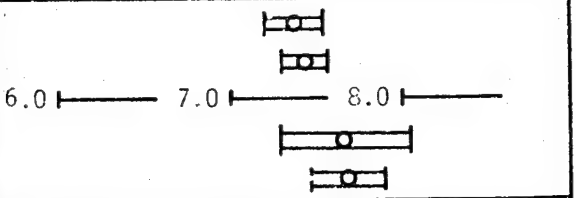
	Wet		7.44 ± 0.14	
Modulus Type II Quasi-static load Rate=20 lb/sec	Wet		7.68 ± 0.39	
	Dry		7.68 ± 0.22	
Modulus Type I G.L.=4 in. Cyclic Load R=0.1 σ_{max}=50 ksi	Dry	Initial	7.55 ± 0.21	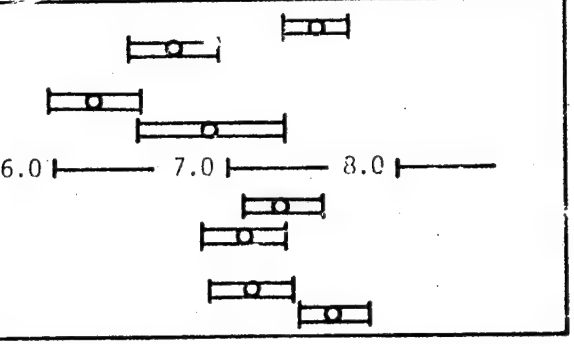
		look	6.70 ± 0.28	
	Wet	look	6.25 ± 0.26	
		Initial	6.90 ± 0.43	
Modulus Type II G.L.=4 in. Cyclic load R=0.1 σ_{max}=50 ksi	Dry	Initial	7.61 ± 0.25	
		look	7.13 ± 0.25	
	Wet	look	7.10 ± 0.31	
		Initial	7.30 ± 0.19	

FIGURE 15. SUMMARY OF MODULI DATA

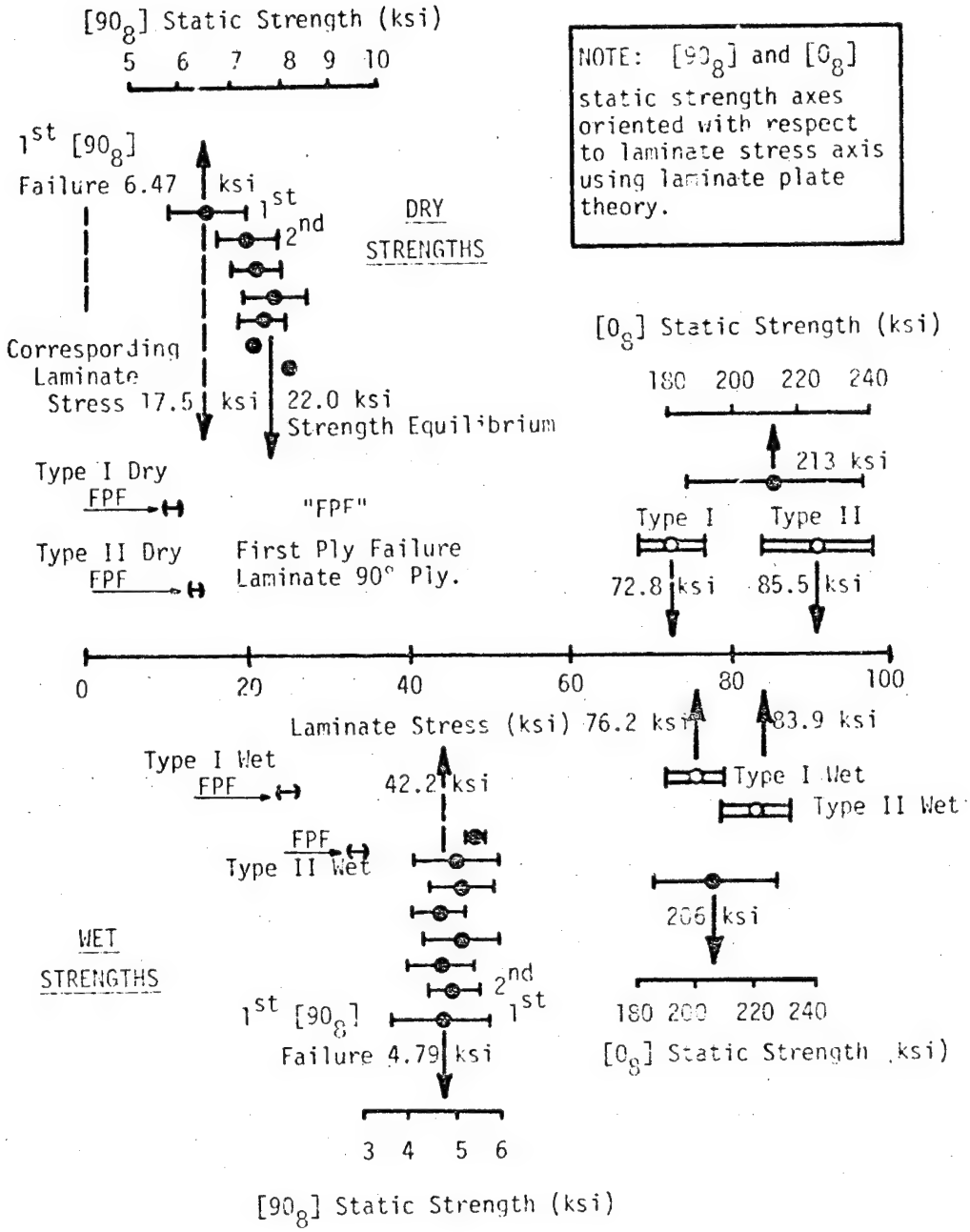

FIGURE 16. CORRELATION OF WET AND DRY [0$_8$] and [90$_8$] STATIC STRENGTHS WITH TYPE I AND TYPE II LAMINATE STRESS STATE AND FIRST 90° PLY FAILURES.

TABLE 10. SUMMARY OF $[90]_8$ WET AND DRY WEAKEST LINK STRENGTHS

Break No.	Dry/Wet Average Strength (ksi)	Wet - Dry Percent Difference	Dry/Wet ± Std. Dev. (ksi)	Dry/Wet No. of Samples
1	6.47/4.47	-27	0.79/1.02	4/6
2	7.34/4.98	-32	0.64/0.48	4/6
3	7.65/4.70	-39	0.60/0.71	4/6
4	7.92/5.14	-35	0.68/0.79	4/6
5	7.68/4.66	-39	0.36/0.58	4/6
6	7.39/5.13	-31	0.10/0.75	3/6
7	8.17/5.03	-38	- /0.87	1/6
8	7.13/5.46	-23	- /0.06	1/2
9	- /5.32	-	- / -	-/1

dry and wet Poisson's ratios, ν_{12}, were determined as 0.313 and 0.315 respectively.

Neither the wet nor dry elastic properties determined from these tests were used in Chapter 3 for predicting the laminate stress state. Properties representative of experimental changes in properties due to wet and dry conditions where chosen, as described in section 3.1, such that the experimental wet value of E_1 was used as a basis for choosing wet and dry elastic properties. These large variations between wet and dry values for E_1, as discussed in section 3.1, are reproduced for the $[0_8]$ tests as shown in Figure 15. A reduction of 9.4 percent in wet transverse modulus, E_2, from the dry state, as shown in Figure 15, is also representative of experimental changes for E_2 as discussed in section 3.1.

Although the experimental elastic properties determined from the unidirectional tests are not used in the stress analysis, the wet and dry strengths are used, as described in section 3.2, to predict the laminate load required for FPF.

The weakest link strength tests for the dry $[90_8]$ specimens appear to reach an equilibrium value, as shown in Figure 14, which is noticably higher than the first dry failure. This same trend is not reproduced in wet strengths which is also graphically demonstrated in Figure 14. The dry and wet $[90_8]$ strengths are graphically referenced with respect to the laminate stress by using laminate theory as shown in Figure 16. It is tempting to relate the experimentally observed FPF plotted in Figure 16 with the first failure measured for

the $[90_8]$ test. Although the graphical correlation of strengths for $[0_8]$, $[90_8]$, type I and type II tests, as shown in Figure 16, is instructive, the correlation of individual failure events should not be assumed since the $[90_8]$ and $[0_8]$ tests are not in the constrained state as are the 90° and 0° plies of a type I or type II laminate. None the less, using the maximum stress theory, as described in section 3.2, justifies comparing the $[90_8]$ strengths and experimental FPF as shown in Figure 16. There are obvious differences in the wet FPF's and first wet $[90_8]$ strength which obviously cannot be justified on the basis of maximum stress theory. This would imply that the edge stresses, which are larger than the interior stresses, may be responsible for the lower FPF's shown in Figure 16. These differences will be discussed in detail in section 4.5.

4.3 Results of Static Tests

4.3.1 Preliminary Quasi-Isotropic Tension Tests

As discussed in the Introduction, previous studies [13,16] have demonstrated that damage which develops along the edge of a type I laminate is different than the damage which develops along the edge of a type II laminate. For wet type I and type II laminates it was shown in section 3.2 that the predicted residual stresses increase the laminate load required to produce FPF. These differences in the predicted wet and dry stresses existing in the laminate interior or along the edge are significant as demonstrated in sections 3.2 and 3.3 and are summarized in Tables 7 and 8. Corresponding differences in edge damage should result from these differences in wet and dry stresses.

The objectives of these static tension tests are to initially isolate unique free edge damage states in wet and dry type I and type II laminates and show how these unique damage states develop into the CDS when the laminate load is increased. Specimens listed in Table 1 were tested as described in section 2.3. The results of these four tension tests are listed in Tables 9 and 11.

As shown in Table 11 there is a substantial difference between the predicted and observed damage in the 90° plies. The predicted values of σ_x, σ_z and N_x^{FPF} which were calculated in sections 3.2 and 3.3 assumed a damage free laminate with all plies having the same thickness. Only trends in damage events are predicted in Table 11 without reference to predicted values of σ_x, σ_z and N_x^{FPF} since the 90° plies in the type I laminate were only one ply thickness and a large amount of initial damage in the type II laminates existed in the form of longitudinal and transverse cracks. For instance, the trend in the damage predicted for type I wet specimen, S12, assumed delaminations would occur as the first damage event followed by transverse cracking since σ_z is much larger than σ_x at the edge (Y/B = 1.0). As a result of these irregularities a detailed comparison between predicted and observed damage is not discussed in this section. The necessary comparisons between predicted and observed damage is discussed in the following section where the test specimens were fabricated with the correct ply thickness and no initial damage.

Although the differences in the predicted damage and experimental

TABLE 11. DAMAGE DEVELOPMENT INTO CHARACTERISTIC DAMAGE STATE FOR PRELIMINARY QUASI-ISOTROPIC TENSION TESTS

Laminate Configuration/ Env. Condition	Item No. (Specimen No.	Predicted 90° Ply Edge Stress State		Unique 90° Damage State		CDS (LL) Prior to Fracture
		σ_x	σ_z	Predicted	Observed (LL)	
$[0/\pm45/90/\mp45/0]_T$/dry	S11	+?	+?	T,FB-D	ID,T(6),FB,D(20)	(27),T,FB-D
$[0/\pm45/90/\mp45/0]_T$/wet	S12	+?	+?	D,FB-T	ID,T(10),ND	(20),T,FB-D
$[0/90/\pm45]_s$/dry	S21	+?	-?	T,ND	ID,T(14),ND	(32),T,FB-D
$[0/90/\pm45]_s$/wet	S22	+?	-?	T,ND	G-ID,T(30),ND	(34),T,FB-D

Symbol Definitions:

σ_x Stress in load direction
σ_z Stress through the thickness
\+ Tension
\- Compression
? Unknown value
Esp Equilibrium Crack Spacing
ID Initial Damage
T Transverse cracks
D Delaminations
I Interface
FPF First ply failure
(LL)(Laminate load, lbs x 100) at which damage occurs
CDS Characteristic damage state

Symbol Prefixes:

G Growth
N No
P Possible
FB Followed by
45 45° ply
90 90° ply

observations are most likely due to the irregularities in fabrication, the damage initially isolated in each test is unique. The growth of these initially unique damage states resulted in the same CDS in the laminate whether wet or dry. The final CDS prior to failure is summarized in Table 11, where the load level, (LL), and description of damage near the fractured region are listed in an abbreviated format. Except for specimen S22, all damage leading to the final fracture was observed to grow from newly formed damage while under load. The final fracture surface of the S22 specimens was observed to grow from initial damage which was observed along the free edge in the 90° and 45° plies prior to the load. The damage, whether induced by the load or existing prior to the load, does not change the crack pattern of the CDS prior to fracture.

Contrary to the irregularities (ply thickness, initial damage) discussed, the preliminary tests provided evidence in the early part of the experimental program that unique damage states followed by growth into the CDS with increasing load could be observed by using the replica technique.

While under a quasi-static tension load all damage eventually grew into the same crack patterns which were characteristic of that laminate (CDS). These patterns grew independently of the uniqueness of the first formation of damage. Even if the growth originated from initial damage due to fabrication there was no appreciable difference in the crack patterns prior to failure. From the results of these preliminary tests the following test and improvements were established:

Using the interactive coaxing technique, described in section 2.5, attempt to coax the first formation of damage (i.e. initial damage due to fabrication) into a final damage state different than the CDS. If the order of occurrence of individual damage events (FPF, equilibrium crack spacing, edge delamination) due to quasi-static or cyclic loads are to be recorded then more replicas should be taken at smaller load intervals.

4.3.2 Development of CDS Due to a Quasi-Static Tension Load

The preliminary tests demonstrated that unique damage states and subsequent growth could be recorded using the replica technique. Unfortunately the stress state predicted in section 3.2 and 3.3 could not be compared with the damage events observed in the preliminary tests due to irregularities detected in the test specimens after fabrication. In this section specimens with no initial damage and correct ply thicknesses are tested as described in section 2.4.

No replicas were taken for the specimens listed in Table 3 which were quasi-statically loaded to fracture. The difference between type I and type II laminate strengths is graphically demonstrated in Figure 14 for both wet and dry conditions which are compared with the experimental dry strengths from reference [14]. When these wet and dry strengths are graphically referenced with respect to the laminate stress state, as shown in Figure 16, the absorbtion of moisture is observed to have reduced the differences between the type I and type II dry strengths. It is interesting to note that a similar reduction in scatter is observed for the wet $[0_8]$ tests also

shown in Figure 16. Since the type I and type II strengths are dominated by the 0° plies these similarities in wet and dry strengths are not surprising. Moduli determined for the wet and dry type I and type II laminates are listed in Figure 15.

As discussed in the introduction the experimental differences between type I and type II laminate strengths provide a basis for investigating how the damage develops under load and influences the laminate strength. As previously noted in section 3.4, understanding how the different CDS crack patterns influence the distribution of stresses prior to fracture is a formidable task which is still under investigation. At best the effort in this section is to demonstrate how the unique damage states due to the wet conditioning affect the CDS as defined in section 3.4.

The last four specimens listed in Table 3 were tested as described in section 2.4 such that first formation of damage and the subsequent growth can be studied and compared with predictions for FPF and crack spacing from section 3.2 and 3.4 respectively. The results of these tests are briefly summarized in Tables 9 and 12.

The predicted value for σ_x and σ_z stresses in the 90° ply as listed in Table 12 are taken from Table 7. The predicted N_x^{FPF}, from section 3.2, are also listed in Table 12 as the laminate load, (LL), shown next to the T designation for 90° ply transverse crack. Although no predictions for the laminate load are made for edge delaminations, the predicted σ_x and σ_z stress would indicate that no delaminations would occur at a lower laminate load for the wet

TABLE 12. DAMAGE DEVELOPMENT INTO CHARACTERISTIC DAMAGE STATE FOR QUASI-ISOTROPIC STATIC TENSION TESTS

Laminate Config./ Env. Cond.	Item No. (Specimen No.)	Predicted 90° Ply* (Edge Stress/ Interior Stresses)		Unique 90° Ply Damage State		CDS (LL)/ Fig. No.
		σ_x (ksi)	σ_z (ksi)	Predict (LL)	Observed (LL)	
Type I/dry	M40 (34)	(9.22/6.27)	(5.25/0)	T(8),FB-D(?)	T(5-6),Esp(12),D(18-20)	(22)/17
Type I/wet	M40 (37)	(9.27/4.55)	(7.64/0)	T(19),FB-D(?)	T(11-12),Esp(17),D(11-12)	(24)/18
Type II/dry	M41 (34)	(8.04/6.27)	(2.87/0)	T(8),ND	T(7-8),Esp(14),ND	(34)/19
Type II/wet	M41 (37)	(6.12/4.55)	(1.71/0)	T(19),ND	T(15-16),Esp(30),ND	(34)/19

*Stresses in 90° ply predicted by FEM with laminate load (800,1900) lb/in choosen such that 90° ply interior stresses are equivalent to wet or dry $[90_8]$ specimen fracture stress.

NOTE: All other symbols defined in Table 11.

conditioned type I laminate.

Although no elevated temperature tests were included in the experimental program, the trend at higher test temperatures for type I wet laminates is to cause the predicted value of σ_x to decrease more than the value predicted for σ_z as temperature is increased with the laminate load held constant. This trend would obviously increase the laminate load required to cause FPF but would lower the laminate load required to cause delaminations. The effect of increasing test temperatures is similar to the effect of swelling due to moisture absorbtion. Higher test temperatures stress relieve the curing stresses. This results in a larger predicted residual value for the compressive wet 90° ply stress, σ_2^R. It may be possible to verify this trend experimentally by testing type I wet laminates at elevated temperatures and show edge delaminations occurring before transverse cracking. Although no elevated temperature tests were performed the swelling of the type I laminate due to moisture experimentally verifies this trend. The observed first occurrence of a wet transverse crack (FPF) occurs between 1100 lb/in and 1200 lb/in which is considerably higher than the first transverse cracks observed in the interval (500-600) lb/in for the dry case. Also the laminate load required to cause delamination has dropped from (1800-2000) lb/in for the dry case to (1100-1200) lb/in for the wet case. Interestingly enough both wet transverse cracks and wet delaminations appear to occur within the same replica load interval of (1100-1200) lb/in, as shown in Figure 17.

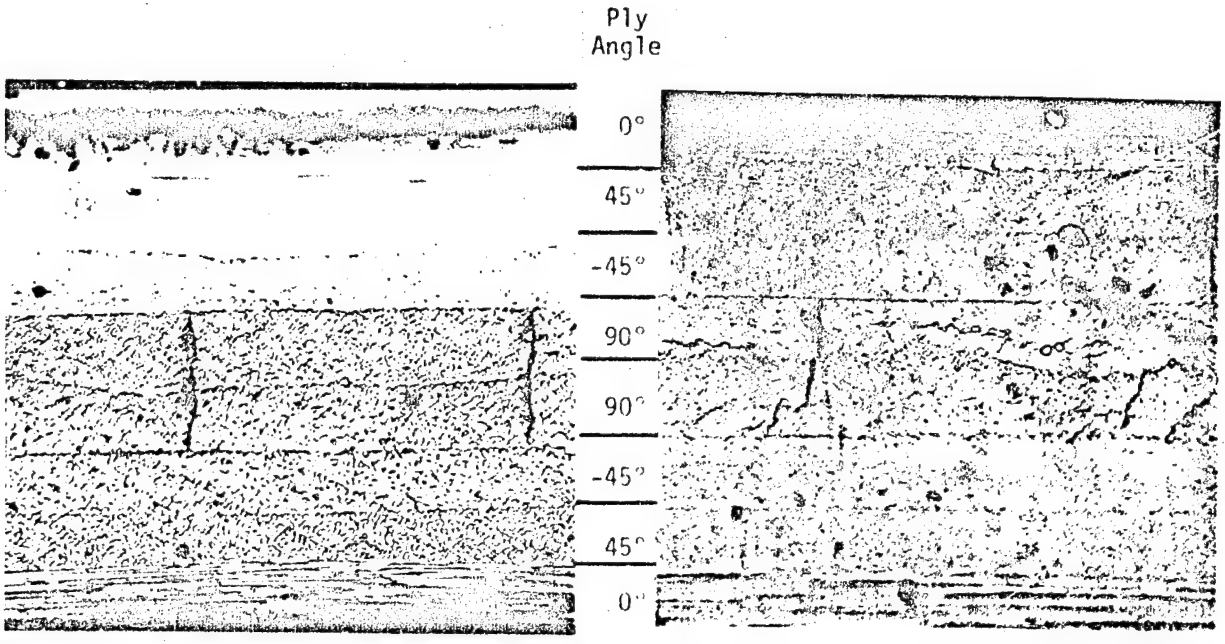

(a) Transverse Cracks Occurring with No Delaminations for a Type I Dry Laminate with N_x=1100 lb/in

(b) Transverse Crack and Delaminations Occurring Simultaneously for a Type I Wet Laminate with N_x=1100 lb/in

FIGURE 17. TRANSVERSE CRACKS AND DELAMINATIONS FOR WET AND DRY TYPE I LAMINATES

A similar trend for the type II wet and dry laminates is not experimentally demonstrated as expected since the predicted value of 2.87 ksi for σ_z in a dry type II 90° ply is larger than the wet value, 1.71 ksi. Both wet and dry values for σ_z are much lower than σ_x at FPF and therefore delaminations are not likely to occur for the type II wet or dry laminates, as is experimentally verified in the replicas shown in Figure 18 and 19 which were taken prior to fracture.

The equilibrium crack spacing in the wet 90° plies for both type I and type II laminates is not affected by the compressive wet residual stress, σ_2^R. As discussed in section 3.5 the residual stresses in the wet laminates only result in increasing the laminate load required for FPF and do not alter the crack spacing of the CDS as defined in section 3.4. The results of the crack spacing are compared with the predicted values listed in Table 9. Due to the simultaneous occurence of delaminations and transverse cracks in the type I wet 90° plies the transverse cracks are not as clearly defined as in the dry condition. The wet type I 90° ply crack shown in Figure 17 appears to be less vertically inclined than the dry transverse cracks and tend to interact with the delaminations resulting in an equilibrium crack spacing which is twice as large as the dry equilibrium crack spacing as shown in Table 9. Both wet and dry equilibrium crack spacing are listed in Table 9 and are compared with predicted crack spacing from section 3.5. In summary the change in the order of damage events due to moisture can obviously affect the

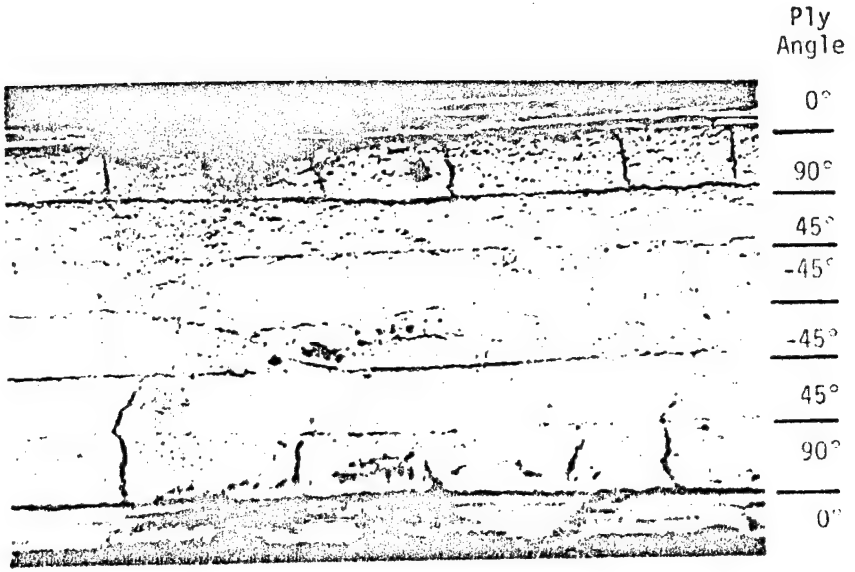

FIGURE 18. FULLY DEVELOPED CHARACTERISTIC DAMAGE STATE FOR TYPE II DRY LAMINATE WITH N_x=3400 LB/IN

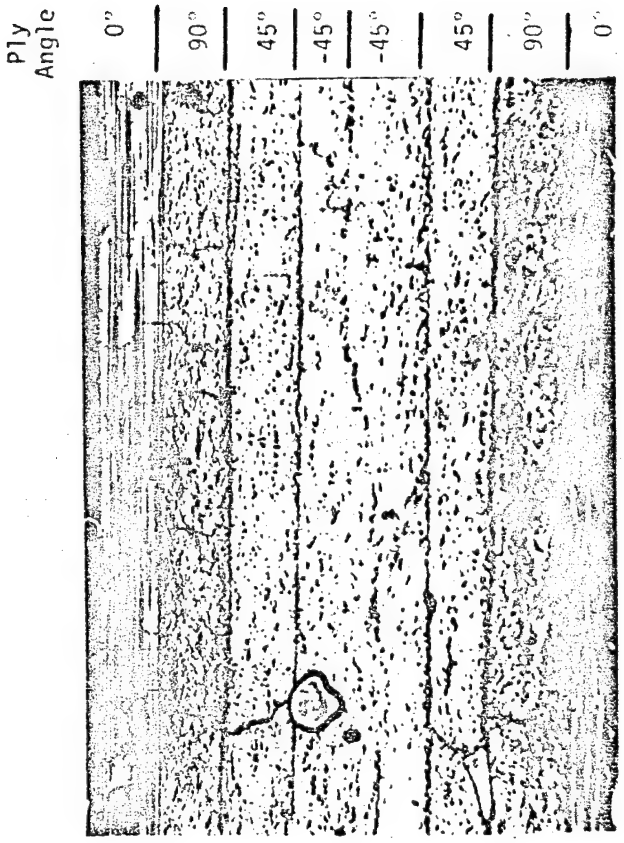

FIGURE 19. FULLY DEVELOPED CHARACTERISTIC DAMAGE STATE FOR TYPE II WET LAMINATE WITH N_x = 3400 LB/IN

equilibrium crack pattern in the 90° ply for the type I laminate.

Although the simultaneous occurrence of delaminations and transverse cracks is the cause of the large crack spacing, the final pattern of cracks recorded at 2200 lb/in for the type I dry and at 2400 lb/in for the type I wet are strikingly similar as shown in Figures 20 and 21, respectively. Small hair like strands extend from the acetate surface when the replica is removed before the acetone has evaporated. When the acetate strip is sandwiched between glass plates for viewing, these hair like strands are seen, as shown in Figure 21, as cracks extending from the delamination cracks. Even though the 90° ply crack pattern is substantially altered in the type I laminate due to moisture absorption, the final crack pattern prior to fracture is not significantly altered. If the characteristic wet and dry crack patterns are similar, it follows that the influence of the wet and dry damaged stress state on the laminate strength should also be similar. This observation is experimentally verified in Table 14 where the average type I laminate dry strength is increased by only 4 percent when 1.2 percent moisture is absorbed. Similarly, the type II wet and dry crack patterns prior to fracture are not substantially different as shown in Figures 18 and 19. In summary, the effect of moisture can significantly alter crack patterns in the type I, 90° plies but the effect on the final CDS and subsequent laminate strength is negligible.

The cracks in the 45° plies were not included when predicting the crack pattern of the CDS as defined in section 3.4. The 45° ply

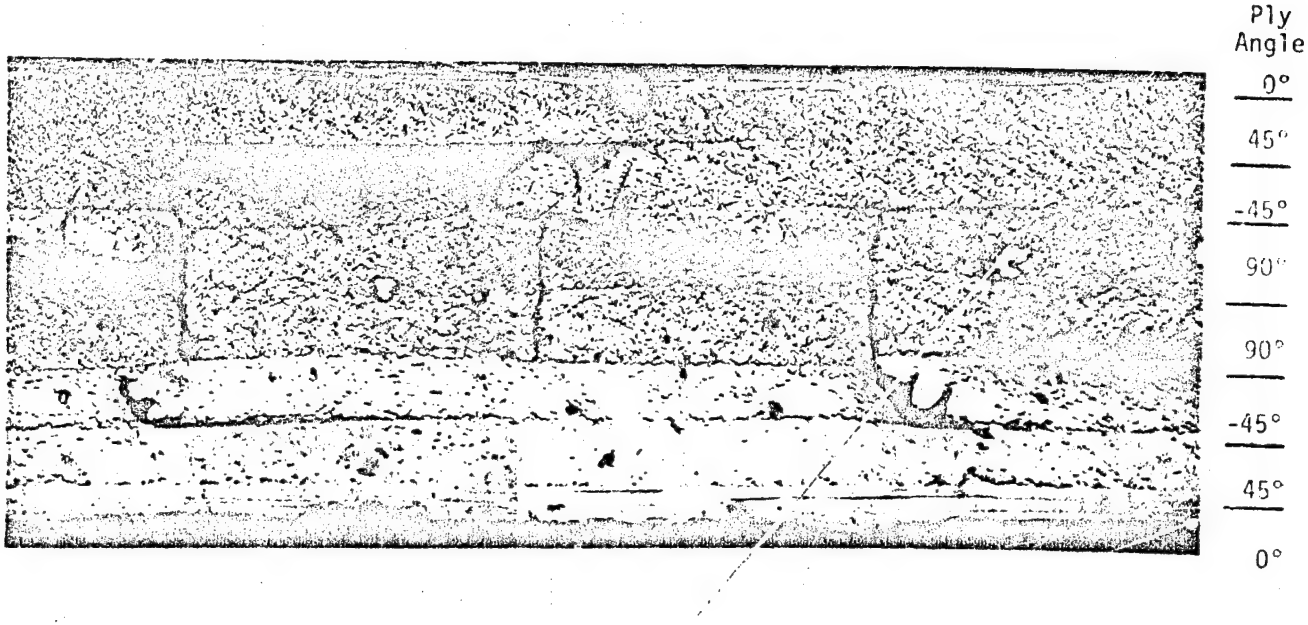

FIGURE 20. FULLY DEVELOPED CHARACTERISTIC DAMAGE STATE FOR TYPE I DRY LAMINATE N_x=2200 LB/IN

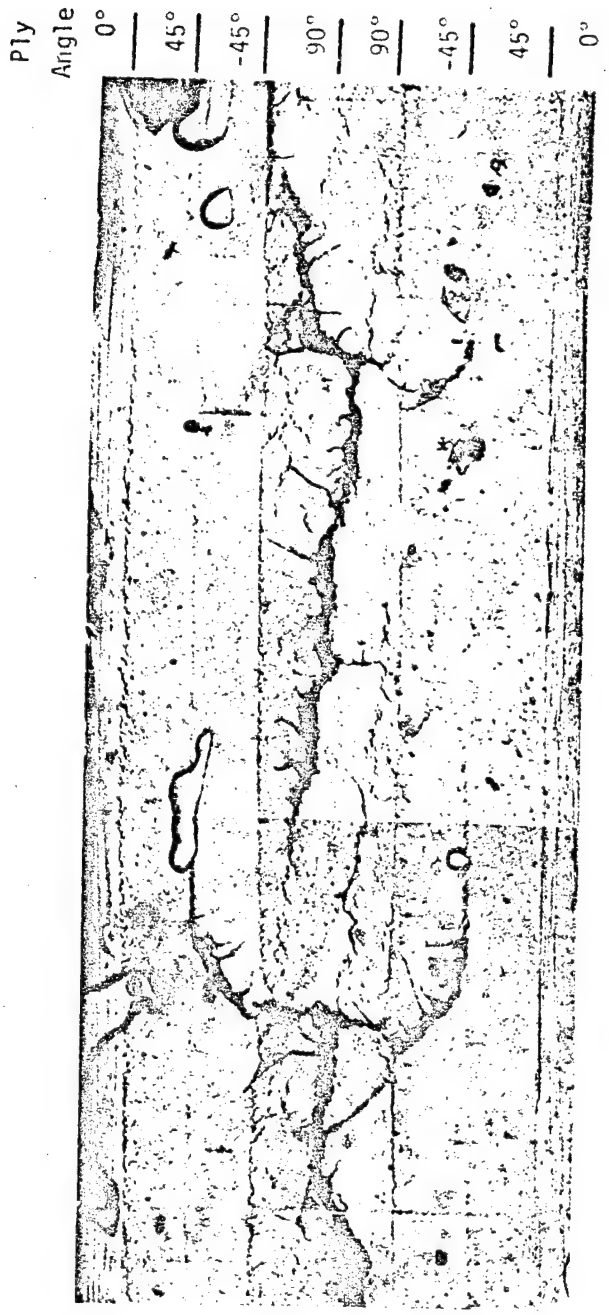

FIGURE 21. FULLY DEVELOPED CHARACTERISTIC DAMAGE STATE FOR TYPE I WET LAMINATE N_x=2400 LB/IN

crack spacing predicted by the shear lag model [16] assumes that the 45° ply crack patterns develop independently of the 90° ply cracks. For wet or dry type I and type II laminates, nearly all 45° ply cracks which develop at the laminate edge appeared to be influenced by transverse cracks in the adjacent 90° plies, as shown in Figures 18 through 21.

4.4 Results of Fatigue Tests

4.4.1 Coaxing Out Different CDS

Four specimens listed in Table 4 were cyclically loaded using the interactive coaxing technique described in section 2.5. The basis for this series of tests was suggested after observing the growth of initial damage along the edge of the preliminary quasi-isotropic tension tests of section 4.3.1.

As previously discussed in section 2.5, there is no clearly defined experimental procedure for the coaxing fatigue tests. The material presented in Chapter III which has been compared with experimental observation in sections 4.3.1 and 4.3.2 provides a better basis at this time on which to outline the following guidelines. As described in section 4.3.1, regardless of the uniqueness of the first formation of damage, all damage developed into the same CDS prior to fracture. This point was reinforced in section 4.3.2 as shown in Figures 18 through 21. The objective of the coaxing tests is not to observe the normal sequence of damage events but to preload the specimens until a unique damage state is observed followed by a cyclic load with a maximum load equivalent to or less then the preload. The

microfiche card reader was used to allow for interpretation of the damage during the test preload. The cyclic load which would peak at or below the preload level would give the existing unique damage an opportunity to grow into a damage state different than the normal sequence of damage events demonstrated in section 4.3.2.

Each of the four laminates listed in Table 4 were preloaded as described in Table 13. The guidelines for each of the four tests are also listed in Table 13. Except for the type I wet test, the guidelines for coaxing the growth of new damage are reasonable when considering the normal sequence of damage events as discussed in section 4.3.2. The inherent nature of the large equilibrium crack spacing for the type I wet laminate was not understood when the coaxing fatigue tests were being conducted. As a result, the higher 2000 lb/in laminate preload was applied and subsequently cycled. A more reasonable preload of 1100 lb/in with a maximum cyclic load of 1000 lbs would have been a wiser choice. This lower cyclic load may have allowed the initial delaminations to grow independently of the initial transverse cracks. As a result, the lower cyclic load may have produced an even larger equilibrium crack spacing than recorded in Table 9 for the type I wet laminate.

The type II wet laminate was preloaded and cycled at a load such that no damage could be observed after the preload. Although no initial damage due to fabrication was present, the growth of microscopic damage in the form of randomly spaced transverse cracks was idealized; but, as shown in Table 13, this unique CDS never

TABLE 13. DAMAGE DEVELOPMENT INTO CHARACTERISTIC DAMAGE STATE FOR THE COAXING FATIGUE TESTS

Laminate Config./ Env. Cond.	Item No. (Specimen No.)	Preload (LL)/ Isolated Damage	Maximum Cyclic Load lbsx100	Quidlines for coaxing Growth of new damage from cyclic load...	Cyclic Damage Growth Observed	Residual Strength (ksi)
Type I/dry	M40 (4)	(16)/T,Esp	16	Without causing 90° ply delaminations	Full Delamin. after 50K	71.4
Type I/wet	M40 (8)	(20)/T,N-Esp	20	Crack spacing below Esp	Crack spacing never reached Esp; CDS at 5K	80.6
Type II/dry	M41 (1)	(18)/Esp, ND, N45T	16	No guidelines	45° cracks grow Indep. of crack in 90° ply	75.9
Type II/wet	M41 (8)	(12)/No damage	10	Such that new damage grows only from ID undetected on edge	No new damage growth is obs. after 2.5M	84.0

NOTE: All symbols defined in Table 11.

materialized, even after 2.5 million cycles. The only coaxing fatigue test that demonstrated a damage event different from the normal sequence was the type II dry. The type II dry specimen was preloaded such that equilibrium spacing was realized with no delaminations, ND, and no cracks in the 45° ply. No guideline was set for the cyclic portion of the test. More 45° ply cracks, as shown in Figure 22, appeared to grow independently of the 90° cracks in the adjacent ply.

Regardless of the guidelines used for coaxing, no large differences in the crack patterns prior to fracture were observed. Except for the type I wet test the residual strengths as listed in Table 13 are not significantly different from the residual strengths listed in Figure 16.

4.4.2 Development of CDS Due to a Cyclic Load

The coaxing cyclic load described in the previous section demonstrated an attempt to coax the growth of damage which was different than the normal sequence observed in the static tension tests. In this section the normal sequence of damage events due to a steady state cyclic load is demonstrated.

All steady state fatigue tests listed in Table 4 were tested as described in section 2.5. All replica specimens were preloaded to 2000 lb in 200 lb load increments followed by a 10 Hz cyclic load at R = 0.1. All remaining steady state fatigue tests which were not replicated were preloaded to 50 ksi followed by a 10 Hz cyclic load at R = 0.1. Replicas and moduli were recorded during the steady

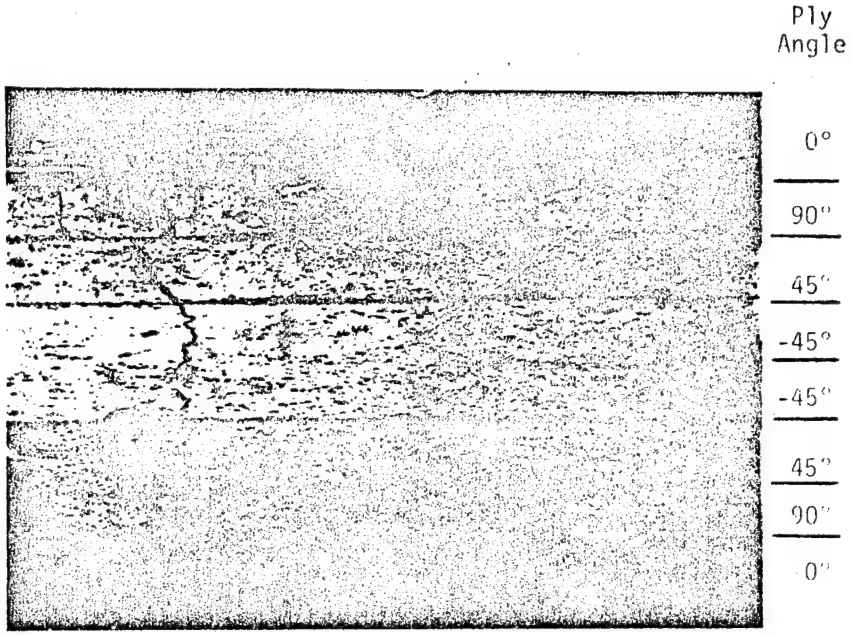

FIGURE 22. COAXING FATIGUE DAMAGE STATE IN A TYPE II DRY LAMINATE AFTER 1 M CYCLES WITH N_x=3200 LB/IN

TABLE 14. DAMAGE DEVELOPMENT INTO CHARACTERISTIC DAMAGE STATE FOR THE STEADY STATE CYCLIC FATIGUE TESTS

Laminate Config./ Env. Cond.	Item No. (Specimen No.	Preload 2000 lbs Damage State Observed (LL)	Max. Cyclic Load 2000 lbs Cyclic Damage Growth Observed (cycles)	Residual Strength/Cycles (ksi)
Type I/dry	M40 (5) M40 (6) M40 (7)	T(4-6), FB-D(18) T(4-8), FB-D(16-20) T(4-6), FB-D(16)	Full D(50K) Full D(2K) Full D(2K)	61.4/1M 69.0/1M 76.8/1M
Type I/wet	M40 (9) M40 (10) M40 (11)	T(8-12), FB-D(8-12) T(8-12), FB-D(8-12) T(8-12), FB-D(8-12)	Full D(2K) Full D(2K) Full D(2k)	57.6/1M 75.7/100K 78.9/1M
Type II/dry	M41 (2) M41 (3) M41 (4)	T(6-8), ND ID,-45T, Two cracks ID,-45T, Four cracks	45T(2K),-45T(10K),-45D45(50K) 45T(5K),-45T(10K),-45D45(100K) -	76.1/100K 76.2/100K 70.6/1M
Type II/wet	M41 (5) M41 (6) M41 (7)	T(14-16), ND T(12-16), ND T(12), ND	45T(50K) 45T(2K),-45D45(50K),-45T(100K) 45T(2K),-45T(50K),-45D45(100K)	80.5/100K 71.3/1M 74.6/100K

Symbols: 45T Transverse cracks in 45° ply
-45T Transverse cracks in -45° ply
-45D45 Delaminations between 45° and -45° plies

NOTE: All other symbols defined in Table 11.

state fatigue tests as outlined in Table 4. Results of the replica steady state fatigue tests are summarized in Table 14. Results of the steady state fatigue tests with no replicas are summarized in Figures 14 and 16.

A brief summary of the edge damage development as observed on replicas due to the preload followed by a steady state cyclic load is presented in Table 14. During the preload of type I dry and wet tests, transverse cracking and delaminations occurred at laminate load levels (LL) similar to LL reported for the static tension tests in Table 12. Only 2000 cycles (2K) were required to grow the initially formed delaminations into a single delamination, "full", running the length of the laminate. Although the higher predicted value for the wet σ_z as discussed in section 4.3.2 is responsible for delaminations occurring sooner during the preload, these same arguements can not be used to predict that the wet delaminations should grow faster when cyclically loaded. For both wet and dry type I laminates, delaminations grow into the fully developed state after the same number of cycles. This would imply that the damaged stress state differs considerably from the undamage state with reference to σ_z near the edge.

The damage resulting from preloading wet and dry type II laminates occurs at loads similar to those reported in Table 12. No delaminations occur in the type II 90° plies during the preload or cycling. Transverse cracking in wet or dry 45° plies of the type II laminates results from the cyclic load and, in most cases observed,

occurs after the same number of cycles. In general, delaminations between the +45 and -45° plies of the type II wet laminate occurs after a larger number of cycles when compared to the type II dry laminate. Damage in the wet and dry type I 45° plies was not recorded due to large delaminations which occurred at approximately 2500 lbs. These large delaminations did not allow for accurate replication of edge damage.

The final and most important observation was that the final recorded damaged crack patterns of the CDS were not significantly altered by the wet or dry conditioning. As a result the residual strengths of the nonreplicated test specimens listed in Figure 16 demonstrate negligible variations due to wet or dry conditioning.

A summary of results for the nonreplicated steady state fatigue tests are listed in Tables 14 and 15. Not only are the differences small between wet and dry residual strength after 100 K cycles but, as compared in Figure 14, the difference in residual and static strengths are small. These same observations are not true for changes in static or cyclic moduli due to wet or dry conditioning, as shown in Figure 15. The trend after a 100 K cycles is demonstrated as a larger change of moduli for the wet and dry type I laminates, with the smallest change in moduli occurring after 100 K cycles for the type II dry laminate.

4.5 Comparison of Stress Analysis with Experimental Observations

As shown in Table 12 and Figure 16 there are obvious differences between dry and wet experimental laminate loads (N_x) required to

produce the first transverse cracks in the 90° plies as observed on the acetate strips. Although the data is scattered due to the load increments over which replicas are taken, a trend is evident between the wet and dry type I and type II laminate loads (N_x) required to produce First Ply Failure (FPF) in the 90° plies. The difference between N_x^{FPF} for type I wet and type II wet is greater than the difference between N_x^{FPF} for type I dry and type II dry. Investigations by Kim and Hahn [11] have shown differences between the dry and wet type I laminate FPF load but these were attributed only to the interior residual stress state as predicted by two-dimensional laminate plate theory.

It is particularly interesting that the differences between type I and type II dry laminate FPF loads is larger for the same laminates in the wet condition. This trend is not surprising when we recall the through the thickness σ_x and σ_z stress distributions near the laminate free edge (Y/B=0.998) as shown in Figure 12. In Figure 12 there is an obvious difference between the interior and edge σ_x and σ_z stresses in the 90° plies for the four laminates. The differences between the interior and edge σ_x and σ_z stresses for the type I wet laminate is much greater than the difference between the same interior and edge stresses in the type II wet which is at the same laminate load (N_x). The difference in 90° ply interior and edge stresses for type I wet laminate is also larger than the differences shown for the type I and type II dry laminates which are at lower laminate loads.

These predicted trends in the stress concentrations of σ_x and σ_z

near the laminate edge as shown in Figure 12 could be used as a basis for explaining the differences previously noted in the experimental data. It is tempting to use these predicted edge stress states together with some failure criterion in order to explain the experimental differences in N_x^{FPF} as previously discussed. Values of the free edge stresses predicted by finite element models are approximations. Crossman [10] points out that only trends in the predicted stress state can be utilized since approximations are made for properties in the lamina 2-3 plane. Also the magnitude of σ_z or σ_x is questionable at the free edge, Y/B=1.0, since the composite material can no longer be modeled as behaving as a homogeneous material one or two fiber diameters from the free edge. With these peculiarities in the stress state established, it is with great caution that the author proposes the following model which will be used to predict FPF in 90° plies for any laminate.

The proposed model assumes that first ply failure initiates in the 90° ply near the laminate free edge since the values predicted for σ_x and σ_z in the 90° ply are larger near the free edge then in the laminate interior. Although more accurate predictions of σ_x and σ_z stresses are obtained in this dissertation by using better approximations for the elastic properties in the lamina 2-3 plane, these improvements in predicting σ_x and σ_z stresses are still incomplete from a continuum viewpoint near the edge. A model is needed which can predict failure without reference to an exact prediction of an experimental stress near a stress concentration. Whitney and Nuismer

[41] point out that determining the strength of a material from the maximum stress at a point is questionable, especially when the maximum stress is highly localized. Whitney and Nuismer further show that the localized nature of a stress concentration near a hole of radius, R, in any quasi-isotropic laminate can be empirically modeled by evaluating a characteristic distance, d_0, from the elasticity solution (34), where the stress ratio $\sigma_y/\bar{\sigma}$ in equation (34) is redefined in terms of experimental notched, σ_N, and unnotched, σ_0, laminate strengths.

$$\sigma_y(\xi)/\bar{\sigma} = 2/(2+\xi^2+3\xi^4) \approx \sigma_N/\sigma_0 \qquad (34)$$

where

$\xi = R(R+d_0)$

R = Hole radius

σ_y = Stress near the stress Concentration

$\bar{\sigma}$ = Far-field stress

σ_N = Notched Strength

σ_0 = Unnotched Strength

d_0 = Characteristic distance from stress concentration

In summary Whitney and Nusimer demonstrate that although a critical stress at some distance, d_0, is the cause of some lower laminate strength, the changes in experimental strengths, σ_N, can be predicted for different hole radii, R, without predicting an experimental value for this critical stress.

Although these stress concentrations were modeled near holes in

quasi-isotropic laminates, the same philosophy can be extended to stress concentrations in individual plies near the laminate free edge. The objective of the proposed model is to predict failure in the 90° ply without reference to predicting an experimental stress near the stress concentration. In the 90° ply, the stress concentration near the laminate edge is not as easily modeled as the stress concentration near a hole in an isotropic plate. Consequently there is no closed form solution predicting σ_x and σ_z in the 90° ply as a function of the distance from the stress concentration since σ_x and σ_z are predicted from a finite element model. We do not require that the predicted stress state near the laminate edge at some distance, a_0, must be numerically equal to the actual stress state at that point. We only require that the variations of σ_x and σ_z at some point near the edge due to variations in stacking sequence together with wet or dry conditioning be realistically predicted by the finite element model. The point at which variations in σ_x and σ_z are to be predicted is not arbitrarily chosen. As suggested by Crossman [10] from a continuum viewpoint the stresses evaluated at five fiber diameters from the edge is more realistic than stresses predicted 7 μm from the edge. Although there is no closed form equation for evaluating this distance, the author chooses 7.7 fiber diameters or Y/B=0.998 as a reasonable distance from the edge to evaluate the FPF stress state in the 90° ply for wet or dry type I and type II laminates. When these predicted 90° ply FPF stress states for each case evaluated in this investigation are substituted into the tensor polynomial failure criterion polynomial

of Appendix A together with F_i and F_{ij} listed in Table 15, then the surviving terms of equation (A.2) are written in equation (35). The terms which remain and contribute significantly to the failure function (FF) are in agreement with the work of Herakovich, Nagarkar and O'Brien [42].

$$2\sigma_x/T - 2\sigma_z/T - (\sigma_x/T)^2 - (\sigma_z/T)^2 = ff \qquad (35)$$

where the transverse strengths of the 90° ply in the lamina 2-3 plane are assumed equal ($F_2=F_3=2/T$; $F_{22}=F_{33}=1/T^2$).

The model uses equation (35) to empirically evaluate a parameter T which is representative of the failure state for the 90° ply in any wet or dry stacking sequence. The σ_x and σ_z stresses are predicted by the FEM at Y/B=0.998 using the experimentally measured N_x^{FPF} and the failure function, ff, is assumed 1.0 since cracks in the 90° ply are experimentally observed on replicas when the experimental laminate load N_x^{FPF} is applied to the laminate.

The proposed model does not imply that the σ_x and σ_z stresses predicted at Y/B=0.998 by the FEM, when an experimental N_x^{FPF} is applied, are the same stresses which exist in the material at Y/B=0.998 when FPF occurs. Since the model requires that the FEM accurately calculate variations in σ_x and σ_z due to differences in stacking sequence together with wet or dry conditioning then the transverse strength, T, calculated from σ_x and σ_z is an effective parameter, T_{eff}, and the proposed model is used to show variations in N_x^{FPF} due to variations in stacking sequence together with wet or dry conditioning.

TABLE 15. EFFECTIVE TRANSVERSE EDGE STRENGTHS, LAMINA STRENGTHS AND DEFINITIONS OF F_i AND F_{ij}

Laminate Configuration/ Env. Conditioning	Item Number (Specimen Number)	Laminate Load, N_x^{FPF} Replica Interval lbs x 100	Effective Transverse Strength (ksi)
Type I/dry	M40 (34)	5 - 6	3.35 - 4.00
Type II/dry	M41 (34)	7 - 8	3.86 - 4.10
Type I/wet	M41 (37)	11 - 12	2.37 - 2.71
Type II/wet	M41 (37)	15 - 16	2.26 - 2.50

Definition of F_i and F_{ij} Tensor Polynomial Terms used by Equations in Appendix A

F_1	$F_2=F_3$	F_{11}	$F_{22}=F_{33}$	$F_{44}=F_{55}=F_{66}$	$F_{12}=F_{13}=F_{23}$
$1/L$	$1/T$	$-1/L^2$	$-1/T^2$	$1/S^2$	-0.58×10^{-10} psi

Wet/Dry Lamina Strengths (ksi) Used to Calculate Values for F_i and F_{ij}

Lamina Longitudinal Strength, L	Lamina Transverse Strength, T	Lamina Shear Strength, S
218/206	6/47/4.74	9.8/7.8

If the values of σ_x and σ_z stresses predicted by FEM are the actual stresses in the material and Y/B=0.998 is the point where failure occurs, then T_{eff} is indeed a mechanical property of the laminate. The model used to study trends and differences in this dissertation ascribes no physical significance to T_{eff}, but requires that it be a constant much the same as d_0 was empirically evaluated as a constant. With the character of the parameter T_{eff} established the transverse strength, T, in equation (35) becomes an effective parameter to be solved for as shown below in equation (36).

$$T_{eff} = \sigma_x + \sigma_z \pm \sqrt{(\sigma_x^2+\sigma_z)^2 - \sigma_x^2 - \sigma_z^2} \qquad (36)$$

where σ_x and σ_z are stresses calculated at a distance 7.7 fiber diameters from the laminate edge using the FEM described in Section 3.3.

As noted, the proposed model requires that only those terms listed in equation (35) are numerically significant when calculating a value for ff. Terms listed in (A.2) containing σ_y which are negligible near the edge, become significant as the edge stresses recover to the stress state in the interior of the laminate. Therefore the model as defined in equation (35), is valid over a small distance from the edge. This distance, a_0, cannot be smaller than is realistic from a continuum point of view and cannot be larger than a certain value for which terms other than those listed in equation (35) significantly contribute to ff.

$$l_l \leq a_0 \leq l_u \qquad (37)$$

where l_l is the minimum distance over which the composite material can be modeled as a continuum and l_u is the distance over which the four terms in equation (35) contribute 99.9 percent of the failure function.

Obviously the lower limit is arbitrarily based on individual interpretation of the finite element grid together with the heterogeneous nature of the fiber/matrix material system. The upper limit depends on values assigned to the tensor polynomial coefficients F_i and F_{ij} (i,j=1,2,3) together with the stresses calculated from the FEM. For the laminates studied in this investigation a lower limit of five fiber diameters is chosen. In general the upper limit for the distance, a_0 from the edge must be less than one laminate thickness since the edge stress state has recovered to the interior solution at this distance and other stress components contribute to FF. At Y/B=0.998 or 7.7 graphite fiber diameters from the edge, the stresses calculated from the FEM described in section 3.3 are combined with coefficients F_i and F_{ij} as listed in Table 15. For all wet and dry laminate stress states evaluated at Y/B=0.998 all terms other than those listed in equation (35) contributed less than ±0.1% to the final value of ff. Although a_0 could be more rigorously defined, the value a_0=1-Y/B=0.002 satisfies the present definition expressed in the inequality (37).

The effective transverse strengths listed in Table 15 are calculated as a function of the experimental N_X^{FPF} laminate loads listed in Table 12. The general linear relationships for the N_X^{FPF} laminate loads and the transverse strengths for wet and dry type I and type II laminates are plotted in Figure 23 along with the experimental N_X^{FPF} in order to demonstrate the trend discussed at the beginning of this section. Although the values calculated for T_{eff} in Table 15 are scattered due to the replica load increment, Figure 23 demonstrates

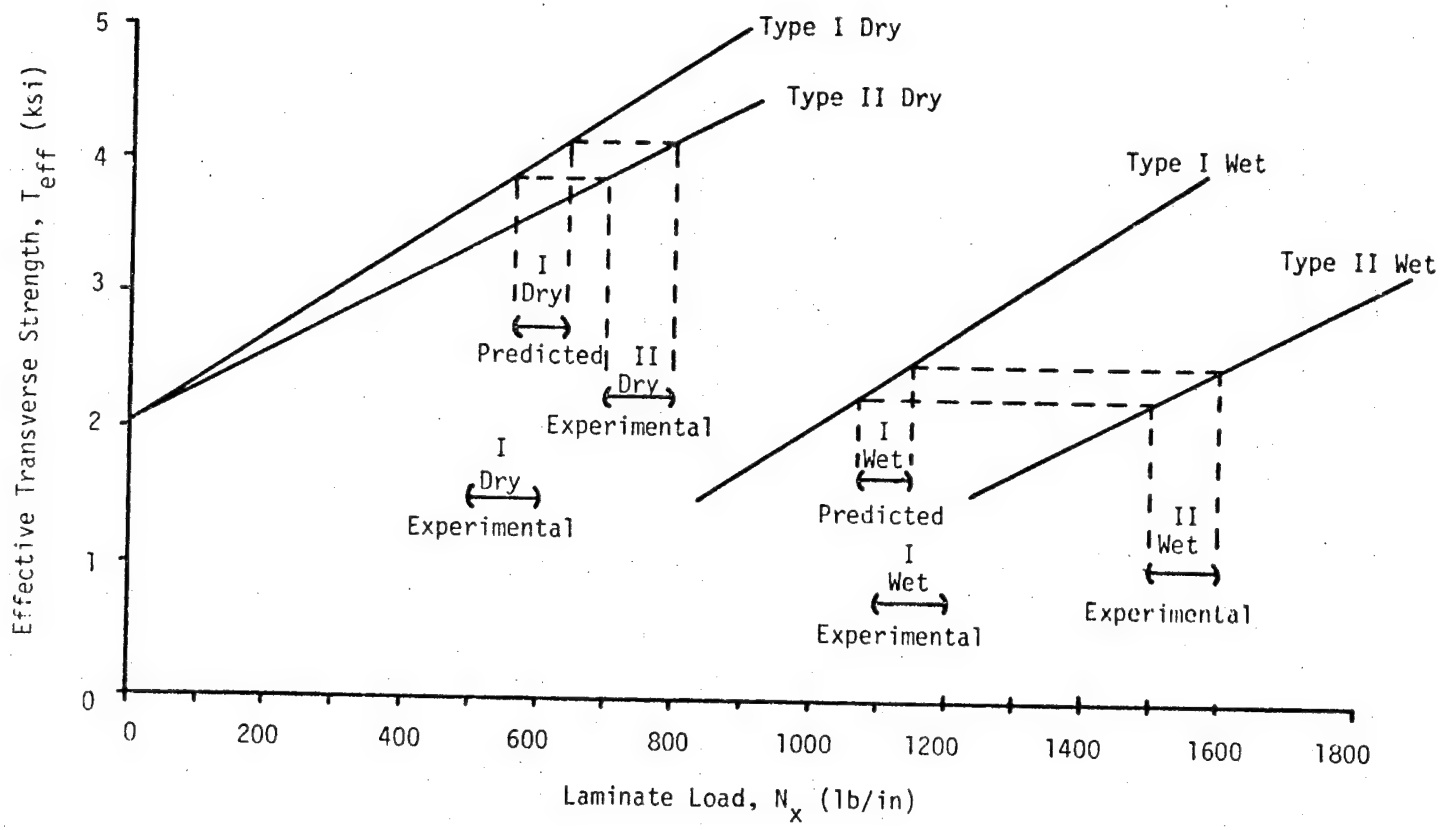

FIGURE 23. COMPARISON OF EFFECTIVE TRANSVERSE EDGE STRENGTHS WITH EXPERIMENTAL OBSERVATIONS

that T_{eff} can be used as a parameter to predict changes in the N_x^{FPF} due to stacking sequence, where T_{eff} for the wet case has a lower value than the T_{eff} for the dry case. The model verifies that the difference between experimental N_x^{FPF} for type I wet and type II wet laminates is larger than the difference between experimental N_x^{FPF} for type I dry and type II dry laminates. Therefore the trend is reproduced by the model and the mechanism responsible for the differences in N_x^{FPF} is due to the variations in values predicted for σ_x and σ_z at Y/B=0.998.

Figure 24 shows a final comparison of the effect that edge stresses have on the laminate load (N_x^{FPF}) required to initiate cracking in the 90° plies. Of particular interest is that type I wet σ_x and σ_z stresses predicted at N_x^{FPF} are nearly equal. A picture of a replica taken at N_x^{FPF} for the type I wet laminate is shown in Figure 17 and demonstrates that both transverse cracking and delaminations occur simultaneously which supports the approximation of equating transverse strengths in the lamina 2-3 plane for wet 90° plies.

In summary, the variations in σ_x and σ_z stresses near the laminate edge are influenced by stacking sequence and environmental conditioning. Variations of σ_x and σ_z stresses in the 90° plies near the edge of wet or dry type I and type II laminates cause the differences in experimental laminate loads required to initiate cracking in the 90° plies. Although the exact magnitude of σ_x and σ_z which initiate transverse cracking and delaminations at the laminate edge are not known, the model developed in this section can relate the experimental laminate FPF loads by

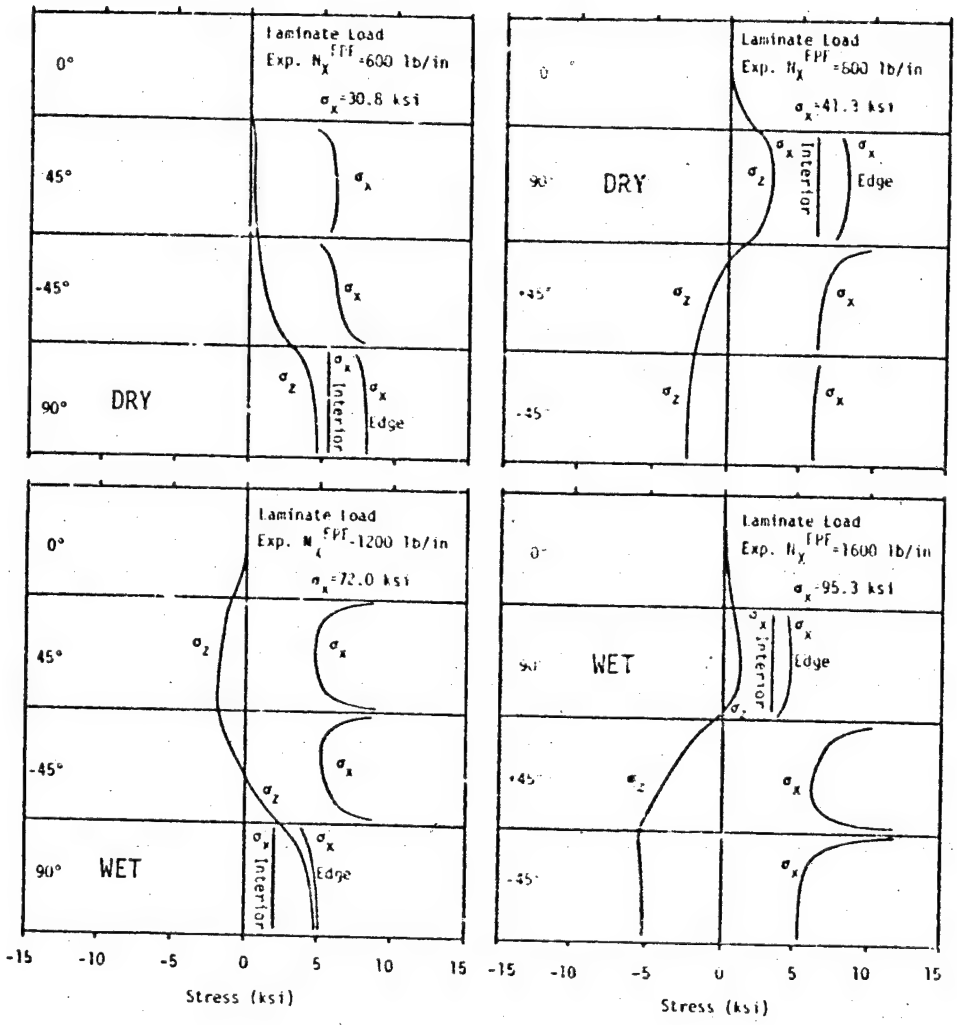

FIGURE 24. FINAL COMPARISON OF σ_x AND σ_z FPF STRESS IN WET AND DRY TYPE I AND TYPE II LAMINATES AT Y/B=0.998

calculating an effective transverse edge strength which is assumed constant within a small region near the laminate edge. Trends and differences of the experimental laminate FPF loads are verified by the model for the wet and dry conditions of type I and type II quasi-isotropic laminates.

V. SUMMARY

The objective of this investigation was to demonstrate the effect of moisture, residual thermal curing stresses and mechanical load on the damage development in quasi-isotropic laminates. In particular this investigation was concerned with demonstrating how the maximum moisture absorbed (wet) in type I and type II laminates, fabricated from T300/5208 graphite/epoxy, significantly alters the dry stress state and subsequent damage development along the laminate edge.

Emphasis is placed on using improved values for wet, dry, and out-of-plane elastic properties since these properties are required to predict the damage free stress state at the laminate edge. Classical laminate theory and a previously developed finite element model (FEM) were used to predict stress states prior to the first formation of damage. Crack patterns characteristic of the laminate in a wet or dry condition were also predicted using a previously developed shear lag model.

Development of edge damage was recorded by using an established replicating technique which transfers an image of edge damage on to a thin acetate sheet. Replicas taken during the test can be immediately viewed on a standard microfiche card reader which allows the experimentalist to interpret the edge damage and interact with the test.

The effect of moisture on $[0_8]$, $[90_8]$, type I and type II test specimens is summarized in Tables 14, 15, and 16. In general moisture tends to reduce the modulus, strength, and scatter of strength for all specimens tested. The difference between the type I and type II

wet strengths is also observed to be less than the difference between type I and type II dry strengths. This decrease in the difference between type I and type II laminate strengths is compared as shown in Figure 16 with the decrease in the scatter of $[0_8]$ strengths when moisture is absorbed. The addition of moisture in the $[90_8]$ tests reduces the first fracture strength from a dry value of 6.47 ksi to a wet value of 4.74 ksi and eliminates the dry strength equilibrium.

The absorbtion of moisture also causes swelling transverse to the fiber direction such that in a type I or type II laminate the residual transverse stress in the 90° ply changes from a dry value of +3.43 ksi to a wet value of -1.96 ksi, as predicted by laminate theory, when 1.2 percent moisture is absorbed. The laminate load which results in the first 90° ply failure (FPF) can be calculated by using the maximum stress theory which assumes FPF occurs when the laminate theory prediction of transverse stress in the 90° ply reaches the $[90_8]$ test specimen strength. As a result of the wet residual compressive stress in the 90° ply, the predicted laminate load required to cause FPF is increased from a dry value of 789 lb/in to a wet value of 1900 lb/in even though the 90° ply strength is reduced due to moisture.

The first occurrence of a 90° ply transverse crack is a single event after which the 90° ply continues to carry a portion of the FPF laminate load. As the laminate load is increased the failure process continues due to the formation of transverse cracks until an equilibrium spacing between cracks is achieved. When equilibrium spacing is obtained the 90° ply no longer carries the σ_x stress due to the applied laminate load.

Moisture was also shown to significantly alter the dry type I laminate edge σ_x and σ_z stresses predicted by the FEM such that delamination would occur at a lower laminate load due to an increase of σ_z when moisture is absorbed. Similarly FPF would occur at a higher laminate load due to a predicted decrease in σ_x when moisture is absorbed. Using the replica technique the first occurrence of wet FPF was observed within the load interval (1100-1200) lb/in which is larger than the FPF laminate load of (500-600) lb/in which was observed for the dry case. Also the laminate load required to cause delaminations was observed to decrease from (1800-2000) lb/in for the dry case to (1100-1200) lb/in for the wet case. As a result of moisture absorbtion, transverse cracks and delaminations were observed to occur simultaneously in the 90° plies of a type I laminate when the laminate load reached (1100-1200) lb/in.

For wet and dry type I and type II laminates, FPF laminate loads were observed to occur at lower values than the FPF laminate loads predicted using the maximum stress theory which considers only the value of the σ_x stress predicted by laminate theory. An improved estimate of FPF laminate loads should include the σ_z and σ_x edge stresses, calculated by an FEM using wet and dry elastic properties, and interlaminar strengths.

For wet or dry laminates there is a difference between the type I and type II FPF laminate loads. The difference between the type I and type II wet FPF laminate loads was larger than the difference between the type I and type II dry FPF laminate loads. A model was

developed which predicted these differences. The model demonstrated that differences in the observed FPF laminate loads were accounted for by the predictable changes in the FEM calculated values of σ_x and σ_z edge stresses which were the result of changes in stacking sequence together with wet or dry environmental conditioning.

The absorbtion of moisture was observed and predicted to have less than a 10 percent increase in the crack spacing between the 90° ply transverse cracks in the type II laminates. For the type I laminate the addition of moisture nearly doubles the distance between 90° ply transverse cracks as a result of delaminations occurring simultaneously and interacting with the transverse cracks.

Although moisture was shown to significantly alter the first formation of damage in the 90° plies, the fully developed crack patterns prior to fracture, which develop from static or cyclic loads, were not significantly altered by moisture. Consequently, the difference between the redistributed stresses in damaged wet and dry laminates prior to fracture will be small; and as a result, these differences will have a negligable effect on the laminate strength. This observation was experimentally verified as small differences between wet and dry laminate residual or static strengths.

VI. CONCLUSIONS

In general moisture tends to reduce moduli, strengths, and scatter of strength for $[0_8]$, $[90_8]$, $[0/\pm45/90]_s$ and $[0/90/\pm45]_s$ specimens fabricated from T300/5208 graphite-epoxy. Moisture also reduces the difference between type I, $[0/\pm45/90]_s$, and type II, $[0/90/\pm45]_s$, laminate strengths. The dry equilibrium strength, which is experimentally observed for the dry $[90_8]$ tests, is eliminated when moisture is absorbed.

The first formation of edge damage such as first 90° ply failures (FPF) and delaminations can be recorded by using an established replica technique. Damage recorded on replicas taken during the test can be immediately viewed on a standard microfiche card reader such that the development of edge damage can be conveniently interpreted during the test.

Moisture was observed to significantly alter the dry type I laminate edge residual stress state predicted by a FEM such that delaminations would occur at a lower laminate load and FPF would occur at a higher laminate load. These predicted trends due to moisture absorbtion were experimentally verified using the replica technique.

For the type I wet laminate delaminations were observed to occur simultaneously and interact with transverse cracks in the 90° plies such that the equilibrium spacing was twice the value observed for the type I dry laminate.

The absorbtion of moisture was observed and predicted to have less

than a 10 percent increase in the equilibrium crack spacing in the 90° plies of the type II laminate.

By using the model developed in this investigation it is possible to predict changes in FPF laminate loads due to differences in stacking sequence together with wet or dry environmental conditioning. These differences in FPF laminate loads were accounted for by the predictable change in the FEM calculated values of σ_x and σ_z edge stresses due to changes in stacking sequence together with wet or dry environmental conditioning.

Although moisture content affects the load at which damage initiates in graphite epoxy laminates, the complete damage state which develops from static and cyclic loads prior to fracture is a characteristic of the laminate stacking sequence and is not a function of loading history (monotonic or cyclic loads) and environmental conditioning (wet or dry). For the laminates and conditions examined in this investigation, the experimental data show that the tensile strength of monotonically loaded specimens and the residual tensile strength of cyclically loaded, fully damaged, specimens are dependent on stacking sequence and are independent of the hygro-mechanical history of specimens with the same stacking sequence. The results suggest that strength of a composite laminate is not influenced by the details of individual damage events but rather is dependent on the collective form of the various damage details as described by the concept of a damage state which is a laminate property and how the damage state affects the strength state of a laminate.

VII. REFERENCES

1. Browning, C. E., Husman, G. E. and Whitney, J. M., "Moisture Effects in Epoxy Matrix Composites," Composite Materials: Testing and Design (Fourth Conference), ASTM STP 617, American Society for Testing and Materials, 1977, pp. 481-496.

2. Unnam, J. and Tenny, D. R., "Analytical Prediction of Moisture Absorption/Desorption in Resin Matrix Composites Exposed to Aircraft Environments," Presented at the AIAA-ASME 18th Structures, Structural Dynamics and Materials Conference, AIAA Paper No. 77-400.

3. Kaelble, D. H., Dynes, P. J., Crane, L. W. and Maus, L., "Interfacial Mechanisms of Moisture Degradation in Graphite-Epoxy Composites," J. Adhesion, Vol. 7 (1975) pp. 25-54.

4. Augl, J. M. and Berger, A. E., "Moisture Effect on Carbon Fiber Epoxy Composites," SAMPE Technical Conference, Vol. 8 (1976) pp. 383-427.

5. Miller, A. K. and Adams, D. F., "Inelastic Micromechanical Analysis of Graphite/Epoxy Composites Subjected to Hygrothermal Cycling," Advanced Composite Materials - Environmental Effects, ASTM STP 658, J. R. Vinson, American Society for Testing and Materials, 1978, pp. 121-142.

6. Shen, C. H. and Springer, G. S., "Environmental Effects on the Elastic Moduli of Composite Materials," J. Composite Materials, Vol. 11 (1977), p. 250.

7. Shen, C. H. and Springer, G. S., "Moisture Absorption and Desorption of Composite Materials," J. Composite Materials, Vol. 10 (1976), p. 2.

8. Browning, C. E., "The Mechanisms of Elevated Temperature Property Loses in High Performance Structural Epoxy Resin Matrix Materials After Exposures to High Humidity Environments," SAMPE Symposium, Vol. 22 (1977) p. 365.

9. Shirrel, C. D., Leisler, W. H. and Sandow, F. A., "Moisture-Induced Surface Damage in T300/5208 Graphite-Epoxy Laminates,"

10. Crossman, F. W., Mauri, R. and Warren, W., "Hygrothermal Damage Mechanisms in Graphite-Epoxy Composites, Final Report No. LMSC-D626480," June 1978, Lockheed Palo Alto Research Laboratory Lockheed Missiles and Space Co., Inc., Palo Alto, Calif.

11. Kim, R. Y. and Hahn, H. T., "Effect of Curing Stresses on the First Ply-Failure in Composite Laminates," J. Composite Materials, Vol. 13 (1979), p. 2.

12. Pagano, N. J. and Pipes, R. B., "Some Observations on the Interlaminar Strength of Composite Laminates," Int. J. Mech. Sci., Vol. 15 (1973) pp. 679-688.

13. Stalnaker, D. O., "An Investigation of Edge Damage Development in Quasi-Isotropic Graphite-Epoxy Laminates," Thesis, Dept. of Engineering Science and Mechanics, School of Engineering, Virginia Polytechnic Institute and State University, (April 1976).

14. Crossman, F. W., "Analysis of Free Edge Induced Failure of Composite Laminates," Proceedings of US-USSR Conference on Fracture of Composite Materials, Riga, Latvia, USSR, Sept., 1978.

15. Whitney, J. M. and Kim, R. Y., "Effects of Stacking Sequence on the Notched Strength of Laminated Composites," Composite Materials: Testing and Design (Fourth Conference), ASTM STP 617, American Society for Testing and Materials, 1977, pp. 229-242.

16. Reifsnider, K. L., Henneke, E. G., and Stinchcomb, W. W., "Defect-Property Relationships in Composite Materials," Technical Report AFML-TR-75-81, Part III, June, 1978.

17. Reifsnider, K. L. and Masters, J. E., "Investigation of Characteristic Damage States in Composite Laminates," presented at winter Annual Meeting, San Francisco, Calif., Dec. 10-15, 1978, ASME, Preprint No. 78-WA/Aero-4.

18. Dean, G. D. and Turner, P., "The Elastic Properties of Carbon Fibers and Their Composites," Composites, July, 1973.

19. Ishikawa, T., Koyama, K., and Kobayashi, S., "Elastic Moduli of Carbon-Epoxy Composites and Carbon Fibers," J. Composite Materials, Vol. 11 (July 1977), p. 332.

20. Kriz, R. D. and Stinchcomb, W. W., "Elastic Moduli of Transversely Isotropic Graphite Fibers and Their Composites," Experimental Mechanics, Vol. 19, No. 2, Feb. 1979, pp. 41-49.

21. Long, E., via private communication, Engineer Mat'l. Res. Brnch. NASA Langley, Hampton, Va.

22. Lindrose, "Ultrasonic Wave and Moduli Changes in a Curing Epoxy Resin," Experimental Mechanics, June 1978, pg. 227.

23. Rybicki, E. F. and Schmueser, D. W., "Three Dimensional Finite Element Stress Analysis of Laminated Plates Containing a Circular Hole," AFML-TR-76-92 (Aug. 1976).

24. Pipes, R. B. and Pagano, N. J., "Interlaminar Stresses in Composite Laminates under Uniform Axial Extension," J. Comp. Materials, Vol. 4 (1970), p. 538.

25. Hsu, P. W. and Herakovich, "Interlaminar Stresses in Composite Laminates -- A Perturbation Analysis," Virginia Polytechnic Institute and State University, VPI-E-76-1, Jan., 1976.

26. Kriz, R. D., "Effect of Material Properties on Interlaminar Stresses in Angle-Ply Composite Laminates," Virginia Polytechnic Institute and State University, VPI-E-77-16, March, 1977.

27. Hashin, Z., "Theory of Fiber Reinforced Materials," NASA-CR-1974 (March 1972).

28. Hahn, H. T. and Kim, R. Y., "Swelling of Composite Laminates," Advanced Composite Materials - Environmental Effects, ASTM STP 658, J. R. Vinson Ed., American Society for Testing and Materials, 1978, pp. 98-120.

29. Hofer, Jr., K. E., Larsen, D. and Humphreys, V. E., "Development of Engineering Data on the Mechanical adn Physical Properties of Advanced Composite Materials," NTIS #AD-A014 363 (Feb. 1975).

30. Jones, R. M., Mechanics of Composite Materials, McGraw-Hill, New York, 1975, pp. 147-173.

31. Pagano, N. J. and Hahn, H. T., "Evaluation of Composite Curing Stresses," Composite Materials: Testing and Design (Fourth Conference), ASTM STP 617, American Society for Testing and Materials, 1977, pp. 317-329.

32. Nagarkar, A. P. and Herakovich, C. T., "Nonlinear Temperature Dependent Failure Analysis of Finite Width Composite Laminates," Virginia Polytechnic Institute and State University, VPI-E-79-36, Sept., 1979.

33. Herakovich, C. T., Renieri, G. D., and Brinson, H. F., "Finite Element Analysis of Mechanical and Thermal Edge Effects in Composite Laminates," Army Symposium on Solid Mechanics, 1976, Composite Materials: The Influence of Mechanics of Failure on Design, Cape Cod, Ma., Sept., 1976.

34. Humphreys, E. A. and Herakovich, C. T., "Nonlinear Analysis of Bonded Joints with Thermal Effects," Virginia Polytechnic Institute and State University, VPI-E-77-19, June, 1977.

35. O'Brien, D. O. and Herakovich, C. T., "Finite Element Analysis of Idealized Composite Damage Zones," Virginia Polytechnic Institute and State University, VPI-E-78-6, Feb., 1978.

36. Talug, A., "Analysis of Stress Fields in Composite Laminates with Interior Cracks," Dissertation, Dept. of Engineering Science and Mechanics, School of Engineering, Virginia Polytechnic Institute and State University, (Aug. 1978).

37. Garret, K. W. and Bailey, J. E., "Multiple Transverse Fracture in 90° Cross-Ply Laminates of a Glass Fibre-Reinforced Polyester," Journal of Materials Science, Vol. 12, (1977), pp. 157-168.

38. Parvizi, A. and Bailey, J. E., "On Multiple Transverse Cracking in Glass Fibre Epoxy Cross-Ply Laminates," Journal of Materials Science, Vol. 12 (1977), pp. 2131-2136.

39. Zweben, C., "On the Strength of Notched Composites," J. Mech. Phys. of Solids, Vol. 19, 1971, pp. 103-116.

40. Kulkarni, S. V., McLaughlin, P. V., Jr., and Pipes, R. B., "Fatigue of Notched Fiber Composite Laminates," NASA CR-145039, Materials Sciences Corporation, 1977.

41. Whitney, J. M. and Nuismer, R. J., "Stress Fracture Criteria for Laminated Composites Containing Stress Concentrations," J. Comp. Materials, Vol. 8 (July 1974), p. 253.

42. Herakovich, C. T., Nagarkar, A. and O'Brien, D. A., "Failure Analysis of Composite Laminates with Free Edges," ASME Conference, New York, 1979.

APPENDIX A

TENSOR POLYNOMIAL FAILURE CRITERION

APPENDIX A

TENSOR POLYNOMIAL FAILURE CRITERION

The tensor polynomial failure criterion in the contracted tensor notation (for an orthotropic material in the principal material directions) has the form

$$\begin{aligned} &F_1\sigma_1+F_2\sigma_2+F_3\sigma_3+F_{11}\sigma_1^2+F_{22}\sigma_2^2 \\ &+F_{33}\sigma_3^2+F_{44}\tau_{23}^2+F_{55}\tau_{13}^2+F_{66}\tau_{12}^2 \\ &+2F_{12}\sigma_1\sigma_2+2F_{13}\sigma_1\sigma_3+2F_{23}\sigma_2\sigma_3 = 1 \end{aligned} \tag{A.1}$$

where the F_i and F_{ij} terms are as previously defined in Table 15. In the xyz (laminate) coordinate system, the tensor polynomial failure criterion transforms (from the 1-2 to x-y by anticlockwise rotation of $+\theta$) into

$$\begin{aligned} &F'_1\sigma_x+F'_2\sigma_y+F'_3\sigma_z+F'_6\sigma_{xy}+F'_{11}\sigma_x^2 \\ &+F'_{22}\sigma_y^2+F'_{33}\sigma_z^2+F'_{44}\tau_{yz}^2+F'_{55}\tau_{xz}^2 \\ &+F'_{66}\tau_{xy}^2+2F'_{16}\sigma_x\tau_{xy}+2F'_{26}\sigma_y\tau_{xy} \\ &+2F'_{36}\sigma_z\tau_{xy}+2F'_{45}\tau_{yz}\tau_{xz}+2F'_{12}\sigma_x\sigma_y \\ &+2F'_{13}\sigma_x\sigma_z+2F'_{23}\sigma_y\sigma_z = 1 \end{aligned} \tag{A.2}$$

where the F' terms, as functions of the unprimed F's and θ, are as follows ($m = \cos\theta$, $n = \sin\theta$)

$$F'_1 = m^2F_1+n^2F_2$$

$$F'_2 = n^2F_1+m^2F_2$$

$$F'_3 = F_3$$

$$F'_6 = -2mn(F_1-F_2)$$

$$F'_{11} = m^4F_{11}+m^2n^2(F_{66}+2F_{12})+n^4F_{22}$$

$$F'_{22} = n^4F_{11}+m^2n^2(F_{66}+2F_{12})+m^4F_{22}$$

$$F'_{33} = F_{33}$$

$$F'_{44} = m^2F_{44}+n^2F_{55}$$

$$F'_{55} = n^2F_{44}+m^2F_{55}$$

$$F'_{66} = 4m^2n^2(F_{11}+F_{22}-2F_{12})+(m^2-n^2)^2F_{66}$$

$$F'_{16} = -mn[2(m^2F_{11}-n^2F_{22})-(m^2-n^2)(2F_{12}+F_{66})]$$

$$F'_{26} = -mn[2(n^2F_{11}-m^2F_{22})+(m^2-n^2)(2F_{12}+F_{66})]$$

$$F'_{36} = -mn(F_{13}-F_{23})$$

$$F'_{45} = mn(F_{44}-F_{55})$$

$$F'_{12} = m^2n^2(F_{11}+F_{22}-F_{66})+(m^4+n^4)F_{12}$$

$$F'_{13} = m^2F_{13}+n^2F_{23}$$

$$F'_{23} = n^2F_{13}+m^2F_{23}$$

These are transformations from the right handed 1-2 coordinate system into another right hand coordinate system obtained by an anticlockwise rotation of $\theta°$ about the 3 axis. If a ply is oriented at $+\theta°$ from the laminate axis, the F_{ij} are obtained by using the above equations with the sines and cosines of $-\theta°$.

APPENDIX B

ELASTIC LAMINA PROPERTIES

APPENDIX B

ELASTIC LAMINA PROPERTIES

Equations developed by Hashin [27] are listed in terms of fiber and matrix properties denoted by subscripts f and b, respectively. The fiber properties are further denoted by subscripts L and T which correspond to the longitudinal and transverse fiber coordinates defined in Figure 1. Fiber and matrix volume fractions are denoted by V_f and V_b.

The upper and lower bounds for the plane strain bulk modulus in the 2-3 plane shown in Figure 1 are given as

$$K_{23}^{(-)*} = K_b + \frac{V_f}{\frac{1}{K_{f_{TT}} - K_b} + \frac{V_b}{K_b + G_b}} \qquad \text{(a)} \tag{B.1}$$

$$K_{23}^{(+)} = K_{f_{TT}} + \frac{V_b}{\frac{1}{K_b - K_{f_{TT}}} + \frac{V_f}{K_{f_{TT}} + G_{f_{TT}}}} \qquad \text{(b)}$$

Where * indicates the equation used for curve fitting and the (+) and (-) signs indicate upper and lower bounds respectively.

The remaining equations are written using similar notation.

$$G_{23}^{(-)} = G_b + \frac{V_f}{\frac{1}{G_{f_{TT}} - G_b} + \frac{V_b(K_b + 2G_b)}{2G_b(K_b + G_b)}} \qquad \text{(a)} \tag{B.2}$$

$$G_{23}^{(+)*} = G_b \frac{(1+\alpha_1 V_f^3)(\alpha_2+\beta_1 V_f) - 3V_f V_b^2 \beta_1^2}{(1+\alpha_1 V_f^3)(\alpha_2-V_f) - 3V_f V_b^2 \beta_1^2} \qquad (b) \quad (B.2)$$

where

$$\alpha_1 = \frac{\beta_1 - \gamma\beta_2}{1+\gamma\beta_2}, \quad \beta_1 = \frac{1}{3-4\nu_b}, \quad \beta_2 = \frac{K_{f_{TT}}}{K_{f_{TT}} + 2G_{f_{TT}}}$$

$$\alpha_2 = \frac{\gamma+\beta_1}{\gamma-1}, \text{ and } \gamma = G_{f_{TT}}/G_b$$

$$G_{12}^{(-)*} = G_b + \frac{V_f}{\frac{1}{G_{f_{LT}} - G_b} + \frac{V_b}{2G_b}} = G_{13} \qquad (a) \quad (B.3)$$

$$G_{12}^{(+)} = G_{f_{LT}} + \frac{V_b}{\frac{1}{G_b - G_{f_{LT}}} + \frac{V_f}{2G_{f_{LT}}}} \qquad (b)$$

$$E_1 = V_f E_{f_L} + V_b E_b \qquad (B.4)$$

$$E_2 = E_3 = \frac{4K_{23}^{(-)*} G_{23}^{(+)*}}{K_{23}^{(-)*} + \psi G_{23}^{(+)*}} \qquad (B.5)$$

$$\nu_{12} = \frac{V_f E_{f_L} L_1 + V_b E_b L_2 \nu_b}{V_f E_{f_L} L_3 + V_b E_b L_2} \qquad (B.6)$$

$$\nu_{23} = \nu_{32} = \frac{K_{23}^{(-)*} - \psi G_{23}^{(+)*}}{K_{23}^{(-)*} + \psi G_{23}^{(+)*}} \qquad \text{(B.7)}$$

where

$$\psi = 1 + 4K_{23}^{(-)*}\nu_{12}^2/E_1$$

$$L_1 = 2\nu_{f_{LT}}(1-\nu_b^2)V_f + V_b(1+\nu_b)\nu_b$$

$$L_2 = V_f(1-\nu_{f_{LT}} - 2\nu_{f_{LT}}^2)$$

$$L_3 = 2(1-\nu_b^2)V_f + (1+\nu_b)V_b$$

Prof. Donald F. Adams
Dept. Of Mechanical Engineering
University Of Wyoming
Larmie, WY 82070

Dr. M. R. Adsit
General Dynamics Convair
P.O. Box 80837
San Diego, CA. 92138

Dr. J. A. Bailie
D81-12 Bldg. 154
Lockheed Missiles & Space Co,Inc
1111 Lockheed Way
Sunnyvale, CA. 94088

Mr. Henry W. Bergner, Jr.
The Boeing Company
Mail Stop 3707
Seattle, WA. 98124

Dr. Charles W. Bert, Director
School Of Aerospace, Mechanical
& Nuclear Engineering
The University Of Oklahoma
Norman, Oklahoma 73069

Mr. Richard Boitnott
Mail Stop 188a
Nasa-Langley Research Center
Blacksburg, Va. 24061

Mr. David Bowles
Mail Stop 188M
NASA-Langley Research Center
Hampton, Va. 23665

Dr. H. F. Brinson
ESM Dept.
VPI&SU
Blacksburg, VA. 24061

Dr. Richard F. Card
Mail Stop 190
NASA-Langley Research Center
Hampton, VA 23665

Dr. C. Chamis
NASA-Lewis Research Center
2100 Brook Park Rd.
Cleveland, Ohio 44135

Dr. Paul A. Cooper
Mail Stop 190
NASA-Langley Research Center
Hampton, Va. 23665

Dr. Frank Crossman
Lockheed Research Lab
Org. 52-41, Bldg. 204
3251 Hanover Street
Palo Alto, CA. 94304

Dr. I. M. Daniel, Manager
IIT Research Institute
10 West 35 Street
Chicago, IL. 60616

Dr. John B. Davidson
Mail Code 188E
MD-Structural Integrity Branch
Langley Research Center
Hampton, VA. 23665

Dr. John G. Davis, Jr.
Mail Stop 188A
Langley Research Center
Hampton, VA. 23665

Mr. Jerry W. Deaton
Mail Stop 188A
NASA-Langley Research Center
Hampton, VA. 23665

Mr. H. Benson Dexter
Mail Stop 188A
NASA-Langley Research Center
Hampton, VA. 23665

Mr. O. Earl Dhonau
Section 2-53400
Vought Corp.
P.O. Box 5907
Dallas, TX. 75222

Dr. S. C. Dixon
Mail Stop 395
NASA-Langley Research Center
Hampton, VA. 23665

Dr. J. E. Duberg
Mail Stop 103
NASA-Langley Research Center
Hampton, Va. 23665

Dr. M. F. Duggan
52-33/205/2
Lockheed Palo Alto Lab.
3251 Hanover St.
Palo Alto, Ca. 94304

Dr. Wolf Elber
Mail Stop 188E
NASA-Langley Research Center
Hampton, VA. 23665

Mr. Gary L. Farley
Mail Stop 188A
NASA-Langley Research Center
Hampton, VA. 23665

Mr. Larry Fogg
Lockheed-California
Dept. 7572, Bldg. 63, Plant A1
P.O. Box 551
Burbank, CA. 91520

Dr. R. L. Foye
USAMRDL
SAUDLAS (207-5)
Moffet Field, CA. 94035

Dr. D. Frederick
ESM Dept.
VPI&SU
Blacksburg, VA. 24061

Mr. Samuel P. Garbo
McDonnell Aircraft Co.
Bldg. 34, Post 350
St. Louis, MO. 63166

Mr. Ramon Garica
Mail Stop 190
NASA-Langley Research Center
Hampton, VA. 23665

Dr. Login B. Greszczuk
McDonnell Douglas Astr. Co.
5301 Bolas Avenue
Huntington Beach, CA. 92647

Mr. Glen C. Grimes, Engr. Spec.
Structures R & T, Dept 3780/62
Northrop Corp., Aircraft Div.
3901 W. Broadway
Hawthorne, CA. 90250

Dr. H. T. Hahn
Washington University
St. Louis, MO. 63130

Dr. J. C. Halpin
Flight Dynamics Lab
Wright-Patterson AFB
Ohio 45433

Professor Z. Hashin
School of Engineering
Tel Aviv University
Tel Aviv, Israel

Dr. R. A. Heller
ESM Dept.
VPI&SU
Blacksburg, VA. 24061

Dr. E. G. Henneke
ESM Dept.
VPI&SU
Blacksburg, VA. 24061

Professor Phil Hodge
107 Aeronautical Engr. Bldg.
University of Minnesota
Minneapolis, MN 55455

Dr. K. E. Hofer
IIT Research Institute
10 West 35 Street
Chicago, Illinois 60616

Mr. Edward L. Hoffman
Mail Stop 188A
NASA-Langley Research Center
Hampton, VA. 23665

Dr. Peter W. Hsu
Mail Stop 1-1-12
Hamilton Standard Division
Windsor Locks, CT. 06096

Mr. Edward A. Humphreys
Materials Science Corporation
Blue Bell Office Campus
Blue Bell, PA. 19422

Dr. Michael W. Hyer
ESM Dept.
VPI&SU
Blacksburg, VA. 24061

AVCO, Systems Division
Subsystems & Meth. Structures
201 Lowell Street
Wilmington, MA. 01887

Dr. Eric R. Johnson
ESM Dept.
VPI&SU
Blacksburg, VA. 24061

Dr. M. J. Johnson
Mail Stop 226
NASA-Langley Research Center
Hampton, VA. 23665

Dr. M. P. Kamat
ESM Dept.
VPI&SU
Blacksburg, VA. 24061

Dr. Keith T. Kedward
1768 Granite Hills Dr.
El Cajon, CA. 92021

Mr. John M. Kennedy
Mail Stop 188E
NASA-Langley Research Center
Hampton, VA. 23665

Mr. James P. Knauss
Section 2-30400
Vought Corp.
P.O. Box 225907
Dallas, TX. 75265

Dr. Ronald D. Kriz
Dept. Com. NBS Bldg. 2
Boulder, CO. 80302

Dr. S. V. Kulkarni
L342 Lawrence Livermore Lab
P. O. Box 808
Livermore, Ca. 94550

Dr. M. R. Louthan
Materials Engineering
VPI&SU
Blacksburg, VA. 24061

Mr. Vic Mazzio
General Electric Co.
P.O. Box 8555
Bldg. 100, Rm. M4018
Philadelphia, PA. 19101

Mr. Robert R. McWithey
Mail Stop 190
NASA-Langley Research Center
Hampton, VA. 23665

Dr. Martin M. Mikulas
Mail Stop 190
NASA-Langley Research Center
Hampton, VA. 23665

Mr. [illegible]. Steve Mills
6100 Edinger Ave., Apt. 525
Huntington Beach
CA 92647

Dr. D. H. Morris
ESM Dept.
VPI&SU
BLACKSBURG, VA. 24061

Mr. Anya Nagarkar
Material Sciences Corp.
Blue Bell Office Campus
Blue Bell, PA. 19422

NASA Scientific & Technical
Information Facility
P.O. Box 8757
Baltimore/Washington Inter. Air.
Baltimore, MD. 21240

Newman Library - VPI&SU

Mr. David A. O'Brien
5902 Kingsford Pl.
Bethesda, MD 20034

Dr. Donald W. Oplinger
Army Materials & Mechanics
Research Center
Department of the Army
Watertown, MA. 02171

Dr. Nicholas J. Pagano
WPAFB/MBM
Wright Patterson AFB
Ohio 45433

Dr. Nicholas Perrone, Director
Structural Mechanics Program
Department of the Navy
Office of Naval Research
Arlington, VA. 22217

Prof. T. H. H. Pian
Mass. Inst. of Tech.
Dept. of Aero. & Astr.
Cambridge, MA. 02139

Mr. Marek-Jerzy Pindera
Mail Stop 188A
NASA-Langley Research Center
Hampton, VA. 23665

Dr. R. Byron Pipes
Dept. of Mech. & Aero. Engr.
107 Evans Hall
University of Delaware
Newark, DE. 19711

Dr. K. L. Reifsnider
ESM Dept.
VPI&SU
Blacksburg, VA. 24061

Dr. Gary D. Renieri
McDonnell Douglas Astro. Co-East
P.O. Box 516
Bldg. 106, Level 4, Post C-5
St. Louis, MO. 63166

Dr. Michael W. Renieri
McDonnell Aircraft Co.
Bldg. 34, Post 350
St. Louis, MO. 63166

Dr. Larry Roderick
Mail Stop 188E
NASA-Langley Research Center
Hampton, VA. 23665

Dr. B. W. Rosen
Materials Science Corporation
Blue Bell Office Campus
Blue Bell, PA. 19422

Dr. R. E. Rowlands
Dept. of Engineering Mechanics
University of Wisconsin
Madison, WI. 53706

Dr. Edmund F. Rybicki
Battelle
Columbus Laboratories
505 King Avenue
Columbus, OH. 43201

Mr. Harminder Saluja
Boeing Vertol Company
Structural Technology
P.O. Box 16858
Philadelphia, PA. 19142

Dr. J. Wayne Sawyer
Mail Stop 190
NASA-Langley Research Center
Hampton, VA. 23665

Dr. George P. Sendeckyj
Structures Division
Air Force Flight Dynamics Lab.
Wright-Patterson AFB
Ohio 45433

Mr. Mark J. Shuart
Mail Stop 188
NASA-Langley Research Center
Hampton, VA. 23665

Dr. James H. Starnes, Jr.
Mail Stop 190
NASA-Langley Research Center
Hampton, VA. 23665

Prof. Yehuda Stavsky
Gerard Swope Prof. of Mech.
Technion-Israel Inst. of Tech.
Technion City, Haifa, Israel

Dr. W. W. Stinchcomb
ESM Dept.
VPI&SU
Blacksburg, VA. 24061

Dr. Darrel R. Tenney
Mail Code 188M
MD-Materials Research Branch
Langley Research Center
Hampton, VA. 23665

Dr. S. W. Tsai
Nonmetallic Materials Division
Air Force Materials Laboratory
Wright-Patterson AFB
Ohio 45433

Dr. J. R. Vinson
6242 Urey Hall
Applied Mechanics & Science Dept
Univ. of California-San Diego
La Jolla, CA. 92037

Mr. H. E. Waddoups
General Dynamic Corp.
Fort Worth, TX 76101

Dr. T. A. Weisshaar
Aero & Ocean Engr. Dept.
VPI&SU
Blacksburg, VA. 24061

Dr. J. M. Whitney
Nonmetallic Materials Division
Air Force Materials Laboratory
Wright-Patterson AFB
Ohio 45433

Mr. Thomas A. Zeiler
Mail Stop 395
NASA-Langley Research Center
Hampton, VA. 23665

Dr. Carl H. Zweben
General Electric Co.
Space Division
P.O. Box 8555
Philadelphia, PA. 19101

Materials Science Corporation